Metabolic control of primed human pluripotent stem cell fate and function by the miR-200c–SIRT2 axis

HHS Public Access

Author manuscript

Nat Cell Biol. Author manuscript; available in PMC 2017 August 07.

Published in final edited form as:

Nat Cell Biol. 2017 May ; 19(5): 445–456. doi:10.1038/ncb3517.

Metabolic control of primed human pluripotent stem cell fate and function by the miR-200c–SIRT2 axis

Young Cha[1,7], **Min-Joon Han**[1,7,8], **Hyuk-Jin Cha**[2,7], **Janet Zoldan**[3,8], **Alison Burkart**[4], **Jin Hyuk Jung**[1], **Yongwoo Jang**[1], **Chun-Hyung Kim**[1], **Ho-Chang Jeong**[2], **Byung-Gyu Kim**[5], **Robert Langer**[3], **C. Ronald Kahn**[4], **Leonard Guarente**[6], and **Kwang-Soo Kim**[1,9]

[1]Molecular Neurobiology Laboratory, Department of Psychiatry and McLean Hospital, Harvard Medical School, 115 Mill Street, Belmont, Massachusetts 02478, USA

[2]College of Natural Sciences, Department of Life Sciences, Sogang University, Seoul 04107, Korea

[3]Department of Chemical Engineering, David H. Koch Institute for Integrative Cancer Research, MIT, Cambridge, Massachusetts 02139, USA

[4]Section on Integrative Physiology and Metabolism, Joslin Diabetes Center, Harvard Medical School, Boston, Massachusetts 02215, USA

[5]Center for Genomic Integrity Institute for Basic Science, Ulsan National Institute of Science and Technology, Ulsan 44919, Korea

[6]Department of Biology, MIT, Cambridge, Massachusetts 02139, USA

Abstract

A hallmark of cancer cells is the metabolic switch from oxidative phosphorylation (OXPHOS) to glycolysis, a phenomenon referred to as the ‘Warburg effect’, which is also observed in primed human pluripotent stem cells (hPSCs). Here, we report that downregulation of SIRT2 and upregulation of SIRT1 is a molecular signature of primed hPSCs and that SIRT2 critically regulates metabolic reprogramming during induced pluripotency by targeting glycolytic enzymes including aldolase, glyceraldehyde-3-phosphate dehydrogenase, phosphoglycerate kinase, and enolase. Remarkably, knockdown of SIRT2 in human fibroblasts resulted in significantly decreased OXPHOS and increased glycolysis. In addition, we found that miR-200c-5p specifically targets SIRT2, downregulating its expression. Furthermore, SIRT2 overexpression in hPSCs

[9]Correspondence should be addressed to K.-S.K. (kskim@mclean.harvard.edu).

[7]These authors contributed equally to this work.

[8]Present addresses: Department of Hematology, St. Jude Children’s Research Hospital, Memphis, Tennessee 38105, USA (M.-J.H.); Department of Biomedical Engineering, The University of Texas at Austin, Austin, Texas 78712, USA (J.Z.).

AUTHOR CONTRIBUTIONS

Y.C. and M.-J.H.: concept and design, collection and/or assembly of data, data analysis and interpretation, and writing. L.G., H.-J.C. and K.-S.K.: concept and design, data analysis and interpretation, and writing. J.Z., A.B., J.H.J., Y.J. and H.-C.J.: collection and/or assembly of data. C.-H.K., B.-G.K., R.L. and C.R.K.: data analysis and interpretation.

COMPETING FINANCIAL INTERESTS

K.-S.K. is co-founder of NurrON Pharmaceuticals and the remaining authors have no financial conflict to disclose.

Note: Supplementary Information is available in the online version of the paper

significantly affected energy metabolism, altering stem cell functions such as pluripotent differentiation properties. Taken together, our results identify the miR-200c–SIRT2 axis as a key regulator of metabolic reprogramming (Warburg-like effect), via regulation of glycolytic enzymes, during human induced pluripotency and pluripotent stem cell function.

In the early twentieth century, Otto Warburg observed a metabolic switch in transformed cells compared to normal cells from OXPHOS to glycolysis, even in the presence of high levels of oxygen[1,2]. Interestingly, recent studies showed that the metabolism of different types of stem cells, in particular primed pluripotent stem cells (for example, human embryonic stem cells (hESCs) and human induced pluripotent stem cells (hiPSCs)), is also biased towards glycolysis rather than OXPHOS, exhibiting a Warburg-like effect[3–7]. Indeed, more recent studies showed that this metabolic switch from OXPHOS to glycolysis is critical for bioenergetics, biosynthetic capacity, and epigenetic regulation in hPSCs[8–12], which was further supported by metabolomics analyses[11,13]. Unlike hESCs and hiPSCs that represent a primed state, mouse ESCs are known to be at a naive state and energetically bivalent, and can dynamically switch from glycolysis to OXPHOS on demand[9]. Thus, these studies suggest that metabolic reprogramming is intimately linked to stem cell identity during induced pluripotency. However, at present, the molecular mechanism underlying metabolic reprogramming is poorly understood.

Recent proteomics studies revealed that numerous proteins of the nucleus, cytoplasm, and mitochondria involved in diverse aspects of cellular metabolism are highly acetylated in human, mouse, and prokaryotic cells[14–16]. In particular, virtually all enzymes involved in glycolysis and the tricarboxylic acid cycle were found to be acetylated in human liver tissues[15], strongly suggesting that protein acetylation is a keymechanism regulating metabolism[17], which prompted us to hypothesize that protein acetylation regulates, at least in part, metabolic reprogramming. Protein acetylation can be modulated by histone acetyl transferase (HATs), as well as by class I, II, III, and IV histone deacetylases (HDAC). Among these, class IIIHDACs, termed sirtuins, are NAD-dependent protein deacetylases that are highly conserved from bacteria to humans[18,19]. Since sirtuins are the only HDACs whose activity is dependent on NAD, a critical cofactor of cell metabolism, we further hypothesized that certain sirtuin members play important roles in regulating metabolic reprogramming.

Here, we report that altered acetylation levels of glycolytic enzymes by SIRT2 downregulation critically regulate metabolic reprogramming during human induced pluripotency and influence stem cell function and regulation in primed hPSCs.

RESULTS

Warburg-like effect in hPSCs

To compare energy metabolism between hPSCs and their somatic counterpart, we derived hiPSCs from human dermal fibroblasts (hDFs) by introducing four reprogramming genes (c-Myc, Oct4, Sox2, and Klf4) and confirmed pluripotency markers gene expression, almost identical morphology, and pluripotent differentiation potential in the resulting hiPSCs and in

hESCs (Supplementary Fig. 1a–c). In addition, intracellular ATP levels as well as oxygen consumption rate (OCR) were significantly lower in hESCs and hiPSCs compared to hDFs (Supplementary Fig. 1d,e). Since the Warburg effect is closely related to increased glucose uptake by upregulation of glucose transporters (GLUTs) in cancer cells[20], we compared the expression levels of GLUT genes. As shown in Supplementary Fig. 1f, GLUT1-4 mRNAs were significantly upregulated in both iPSCs and hESCs compared to fibroblasts. Taken together, these results, in line with previous findings[11,13,21,22], demonstrate that a Warburg-like effect is operating in primed hPSCs.

Glycolytic enzymes are highly acetylated in hPSCs

To address our hypothesis that acetylation affects the metabolic switch, we compared protein acetylation in hESCs and hDFs by liquid chromatography-tandem mass spectrometry (LC-MS/MS) analyses following immunoprecipitation with acetyl-Lys antibody (Supplementary Fig. 1g). This proteomic analysis identified more than 200 acetylated proteins in both hDFs and hESCs. To minimize non-specificity, we excluded proteins with fewer than 10 peptide hits (black dots, Fig. 1a). The graph in Fig. 1a illustrates this proteomic analysis where proteins with higher acetylation (>1.5 fold) in hESCs (red dots) or in hDFs (blue dots) are shown. We found that a total of 28 and 15 proteins are hyper- and hypo-acetylated in hESCs compared to hDFs, respectively (Supplementary Tables 1 and 2). In agreement with these results, western blot analyses confirmed that hESCs and hiPSCs contain higher levels of acetylated α-tubulin, well-characterized SIRT2 substrate[23], than hDFs, whereas they express similar levels of total α-tubulin (Fig. 1a, inset). Notably, this analysis revealed that 5 out of 10 glycolytic enzymes are hyperacetylated in hESCs: aldolase (encoded by ALDOA), glyceraldehyde-3-phosphate dehydrogenase (encoded by GAPDH), phosphoglycerate kinase (encoded by PGK1), enolase (encoded by ENO1), and pyruvate kinases (encoded by PKM1 and 2) (highlighted in red; Supplementary Table 1). Collision-induced dissociation (CID) spectra of the acetylated peptides derived from these glycolytic proteins are shown in Supplementary Fig. 2.

Downregulation of SIRT2 and upregulation of SIRT1 is a molecular signature of primed hPSCs

We next investigated if any acetylation-modulating factor(s) such as HATs or HDACs show a unique expression pattern in hPSCs compared to their counterpart somatic tissues by means of web-based meta-analyses. We analysed five independent studies of hPSCs against various sets of differentiated cell types (GSE28633; ref. 24, GSE18265; ref. 25, GSE20013; ref. 26, GSE39144 (http://www.ncbi.nlm.nih.gov/geo/query/acc.cgi?acc=GSE39144), and GSE9709; ref. 27) using GEO2R (https://www.ncbi.nlm.nih.gov/geo/geo2r)[28]. We first searched if the expression of any acetyl transferase is consistently altered in hPSCs, but failed to find any in all five meta-analysis studies (Supplementary Table 3). We next analysed all known deacetylases; 11 HDACs (belonging to HDAC I, II, and IV) and 7 SIRTs (belonging to HDAC III). Remarkably, we found that SIRT2 is uniquely and consistently downregulated in all five independent meta-analyses (Supplementary Fig. 3a and Supplementary Table 4). In addition, SIRT1 is upregulated in hPSCs in four meta-analyses. In agreement with this, using another web-based database analysis tool (http://www.nextbio.com), we found that SIRT2 is significantly downregulated whereas SIRT1 is

significantly upregulated in hESCs lines compared to human somatic cells (Fig. 1b and Supplementary Table 5), while expression levels of other sirtuins (SIRT3-7) were variable (Supplementary Fig. 3b–f). These findings prompted us to hypothesize that altered acetylation of metabolic enzymes by SIRT1 and/or SIRT2 plays a critical role(s) in metabolic reprogramming. To test this, we examined their gene expression during induced pluripotency and *in vitro* differentiation. As shown in Fig. 1c,d, SIRT1 and SIRT2 expression (both mRNA and protein level) were prominently up- and downregulated in hPSCs compared to hDFs, respectively, showing that induced pluripotency accompanies SIRT1 induction and SIRT2 suppression. In contrast, during spontaneous differentiation, SIRT2 was highly upregulated whereas SIRT1 was downregulated along with pluripotency markers Oct4 and Sox2 (Fig. 1e). In addition, SIRT2 was robustly upregulated during differentiation of hESCs into midbrain dopamine neurons (Fig. 1g,i), as evidenced by dramatic increases in expression of Tuj1, tyrosine hydroxylase (TH), and Lmx1b (Fig. 1f,g), which was accompanied by a robust decrease in the expression of SIRT1, Oct4 and Nanog (Fig. 1h,i). Our results are in agreement with previous studies showing downregulation of SIRT1 during hESC differentiation[29,30] and upregulation of SIRT2 during mouse ESC differentiation[31].

Functional effects and targets of SIRT2

Because glycolytic enzymes including aldolase, GAPDH, PGK1, enolase, and pyruvate kinases are highly acetylated and the deacetylase SIRT2 is robustly downregulated in hESCs, we hypothesized that SIRT2 downregulation is responsible for their hyperacetylation, directly contributing to the Warburg-like effect. To address this, we generated stable hESC lines in which expression of SIRT2 and EGFP can be induced by doxycycline (Dox) (Fig. 2a and Supplementary Fig. 4a). Under our hESC culture condition using the chemically defined culture medium (E8) containing TGF-β, Dox-induced SIRT2 overexpression (OE) did not change expression levels of pluripotent markers (for example, Oct4, Nanog, Esrrb, and Rex1) or the morphology of hESCs compared to control cells (Fig. 2a and Supplementary Fig. 4b,c). Interestingly, forced expression of SIRT2 in TGF-β-free hESC culture condition resulted in spontaneous differentiation (Supplementary Fig. 4c), which is in line with the Moussaieff *et al.* study showing that inhibition of glycolysis causes a rapid loss of pluripotency in TGF-β-free culture condition[12].

We next investigated the effect of altered SIRT2 expression on acetylation and enzymatic activities of these glycolytic proteins. Remarkably, forced expression of SIRT2 in hESCs prominently deacetylated all four enzymes tested (aldolase, PGK1, enolase, and GAPDH) (Fig. 2b,c), whereas expression levels of their total proteins (see Input; Fig. 2b,c) and mRNAs (Supplementary Fig. 4d) were unchanged. PKM1 and 2 could not be analysed here due to the lack of isoform-specific antibodies. Furthermore, we found that deacetylation of glycolytic enzymes by SIRT2OE in hESCs caused a significant decrease of enzymatic activities for all three enzymes tested (aldolase, enolase, and GAPDH) although the total proteins were unchanged (Fig. 2b–d). SIRT2 bound to aldolase and enolase (Fig. 2e), demonstrating a direct interaction between SIRT2 and these enzymes. Next, we investigated the effect of SIRT2 knockdown (KD) on glycolytic enzymes in hDFs using specific shRNAs. We found that acetylation levels of aldolase, enolase, PGK1 and GAPDH were

substantially increased in SIRT2KD hDFs, although the expression levels of their total proteins were similar (Fig. 2f). Furthermore, their enzymatic activities were significantly increased, demonstrating a direct correlation between their acetylation levels and activities (Fig. 2g).

We next sought to identify specific lysine residues and their functional effects using aldolase (AldoA) as an example. We found that a total of 6 and 8 Lys residues are highly acetylated in mock- and SIRT2KD cells, respectively (Fig. 3a and Supplementary Table 6). Interestingly, K111 and K322 are hyperacetylated in SIRT2KD cells, but not in control cells (Supplementary Fig. 5a–d and Supplementary Table 6). Acetylated and non-acetylated forms of AldoA peptides were well separated and the acetylated form of AldoA was shown to have a 42 higher m/z value due to the acetyl groups. According to protein blast searching (http://blast.ncbi.nlm.nih.gov/Blast.cgi), the K111, but not the K322, residue belongs to the catalytic domain/intersubunit interface (Fig. 3b)[32]. Thus, the K322 residue may represent an as-yet-unidentified domain. In addition, sequence alignment of AldoA showed that K111 and K322 are highly conserved among diverse species (Fig. 3b). To further determine whether K111 and/or K322 are critical for regulating AldoA by SIRT2, we mutated each of them to glutamine (acetylated mimetic) or arginine (deacetylated mimetic) and examined their activity. We found that mutation of K322, but not K111 to Q robustly increased the catalytic activity compared to wild type in both hDFs and 293T cells (Fig. 3c and Supplementary Fig. 5e). Moreover, SIRT2KD prominently activated wild-type AldoA and K111R, but not K322R (Fig. 3d and Supplementary Fig. 5f), demonstrating that K322 deacetylation by SIRT2 significantly downregulates its activity. Notably, the AldoA structure model showed that K322 is exposed to the outside surface of AldoA, suggesting its availability to bind to SIRT2 (crystal structure model of human AldoA, Protein Data Bank code: 1ALD) (Fig. 3e)[33]. Taken together, we propose that SIRT2 directly controls the acetylation levels and enzymatic activities of glycolytic enzymes and contributes to metabolic reprogramming.

SIRT2 expression levels influence metabolism, cell survival, and pluripotent differentiation functions of hPSCs

We next tested if altered SIRT2 levels directly influence glycolytic metabolism in hPSCs by measuring extracellular acidification rate (ECAR)[34]. Indeed, Dox-induced SIRT2OE in H9 hESCs resulted in reduced ECAR and increased OCR levels, compared to control cells (Fig. 4a,b and Supplementary Fig. 6g). The same pattern was observed with H7 hESCs and two independent iPSC lines (for example, hiPSC-1 and hiPSC-2) (Supplementary Fig. 6a–g). Interestingly, the proliferation rate of SIRT2OE hPSCs was significantly reduced compared to control cells (Fig. 4c and Supplementary Fig. 6h). We next performed a fluorescence-based competition assay[35,36]. When wild-type H9 hESCs (WT) were mixed at a ratio of 1:1 with GFP-overexpressing H9 cells (GFP), the ratios of GFP^+/total cells remained 50% up to five passages. In contrast, when WT cells were mixed with SIRT2-GFP-overexpressing H9 cells (SIRT2), the ratio of GFP^+/total cells progressively decreased (Fig. 4d). Since this compromised proliferation/self-renewal capacity can be caused by altered self-renewal per se, cellular senescence or cell death, we next examined the cell population for the presence of the earliest marker of apoptosis, Annexin V. Interestingly, we found that SIRT2OE

significantly increased the apoptotic cell population in all four hPSC lines tested (Fig. 4e,f). In addition, we found that intracellular levels of reactive oxygen species (ROS) were increased by SIRT2OE (Fig. 4g). Furthermore, SIRT2-induced cell death was rescued by pretreatment with *N*-acetyl-*L*-cysteine (NAC), a potent ROS scavenger (Fig. 4h), strongly suggesting that induced SIRT2 levels can cause ROS-dependent apoptotic cell death, leading to compromised proliferation/self-renewal capacity.

Next, we investigated the effect of SIRT2OE on metabolic reprogramming during the early stage of differentiation. We examined mRNA expression patterns for pluripotency and lineage-specific early markers, and measured production of extracellular lactate, a key metabolite of glycolysis. As shown in Fig. 5a–c, SIRT2 expression was prominently upregulated within two days of differentiation along with early-differentiation markers including Pax6, Brachyury (B-T), and Sox17. Furthermore, ECAR levels were decreased as early as three days, while lactate production was significantly reduced at day 4 during *in vitro* differentiation (Fig. 5d,e). Remarkably, we found that Dox-induced SIRT2OE in H9 hESCs and hiPSC-1 during *in vitro* differentiation resulted in a significant reduction of ECAR and extracellular lactate production compared to control cells (Fig. 5d,e and Supplementary Fig. 7a–e). To further determine whether SIRT2 expression levels affect the pluripotent differentiation potential of hESCs, we examined expression patterns for various lineage markers at day 0, 3, 6, 9 or 12 (D0-D12) during spontaneous *in vitro* differentiation. Strikingly, SIRT2OE hESCs with Dox differentiated more efficiently than WT and SIRT2OE without Dox to all three germ layer lineages, as evidenced by staining with antibodies against ectodermal, endodermal, and mesodermal markers (Fig. 5f). Furthermore, expression levels of diverse lineage marker genes of all three germ layers were markedly increased in all four SIRT2OE hPSC lines with Dox compared to WT and SIRT2OE without Dox at all time points tested (D3-D12) (Fig. 5g and Supplementary Fig. 7f). Taken together, our results suggest that SIRT2 levels directly influence energy metabolism and regulate survival and pluripotent differentiation potential of hPSCs.

Expression levels of SIRT2 regulate energy metabolism in hDFs and influence the reprogramming process

We next addressed if proper regulation of SIRT2 expression is critical for induced pluripotency via regulating metabolic reprogramming. To this end, we determined whether altered SIRT2 expression induces a metabolic switch in fibroblasts. Indeed, SIRT2KD in fibroblasts resulted in significant metabolic changes, including decreased OCR and increased ECAR compared to control cells (Fig. 6a,b). Furthermore, compared to control, SIRT2KD cells showed significantly decreased OXPHOS capacity, as evidenced by decreases in basal respiration, ATP turnover, maximum respiration, and oxidative reserve, as well as OCR decrease after FCCP treatment (Fig. 6c–e). We next treated hDFs with reprogramming factors together with SIRT2KD. Notably, reprogramming cells with SIRT2KD showed significantly reduced oxidative metabolism at both day 3 and day 8, compared to control reprogramming cells (Fig. 6f–k). We also examined the dynamics of metabolic change by altered SIRT2 expression during the reprogramming process. As shown in Fig. 7a, 6 days post-transfection of Y4, SIRT2 expression was prominently downregulated. Furthermore, decreased OCR and increased ECAR levels were also

observed as early as 6 days post-transfection, while lactate production was significantly induced at day 9 posttransfection (Fig. 7b–d). Importantly, we found that reprogramming cells with SIRT2KD resulted in significantly enhanced changes in OCR and ECAR levels and induction of extracellular lactate production compared to control reprogramming cells (Fig. 7a–d).

We next tested whether altered SIRT2 expression influences iPSC generation from fibroblasts. Indeed, SIRT2OE in hDFs interfered with iPSC generation by approximately 80% while SIRT2KD significantly increased the efficiency (Fig. 7e,f), suggesting that downregulation of SIRT2 is critical for iPSC generation, via enhancing metabolic reprogramming. In addition, SIRT1KD prominently reduced iPSC generation whereas its overexpression significantly enhanced it (Supplementary Fig. 8e,f), which is in agreement with previous studies[30,37]. However, SIRT1OE with or without reprogramming factors in hDFs did not influence oxidative metabolism at day 3 (Supplementary Fig. 8b–d,g). Notably, SIRT1OE appears to enhance metabolic switch at day 6 (Supplementary Fig. 8h), which is likely due to an indirect effect by enhancing the reprogramming process (Supplementary Fig. 8e,f). To further test whether enhanced reprogramming by SIRT2KD depends on elevated glycolysis, we next tested the effects of 2-deoxy-glucose (2DG), a general inhibitor of glycolysis, on metabolic changes and iPSC generation. Notably, treatment with 0.2 mM 2DG decreased the glycolytic flux in Y4+SIRT2KD to the level of Y4 only without 2DG (Fig. 7h), resulting in the generation of iPSC-like colonies to the level of Y4 only without 2DG (Fig. 7i). In addition, when fibroblasts were treated with 0.5mM 2DG, metabolic changes and increased generation of iPSC-like colonies by SIRT2KD were abrogated (Fig. 7g–i). When fibroblasts were treated with 1mM or higher concentrations of 2DG, the generation of iPSC-like colonies was completely blocked. Taken together, these results strongly suggest that enhanced reprogramming by SIRT2KD is linked to the effect of SIRT2 effect on metabolic reprogramming.

miR-200c suppresses SIRT2 expression

To address whether SIRT2 might be regulated by a specific miRNA(s), we performed miRNA target-prediction analyses using Rna22 (ref. 38) and identified 656 potential miRNAs that can target the SIRT2 gene. Among these, we further identified four hPSC-enriched miRNAs (that is, miR-25, -92b, -200c, and -367) (ref. 39) and their potential target sites (miRNA-response elements; MREs) in the 5′-untranslated region and coding region of SIRT2 (Supplementary Table 7). Interestingly, we found that miR-200c, known to be induced by Oct4 (ref. 40), prominently downregulates SIRT2 expression at both the mRNA and protein levels (Fig. 8a,b). Because our prediction analysis showed that SIRT2 could be targeted by miR-200c-5p but not miR-200c-3p (Fig. 8c and Supplementary Table 7), we determined the effect of each precursor miRNA oligomer on SIRT2 expression. Indeed, pre-miR-200c-5p, but not pre-miR-200c-3p or scrambled oligomers (Scr), significantly decreased the expression level of SIRT2 mRNA or protein (Fig. 8d,e). We also found that pre-miR-200c-5p, but not pre-miR-200c-3p or scrambled sequences, significantly decreased the luciferase reporter expression of both identified MREs (Fig. 8f), indicating that miR-200c-5p downregulates SIRT2 expression by targeting these two MREs. Taken

together, our results support a model in which miR-200c-5p suppresses SIRT2 expression, leading to metabolic reprogramming during human induced pluripotency (Fig. 8g).

DISCUSSION

Here, we uncovered a molecular signature consisting of SIRT2 downregulation and SIRT1 upregulation in primed hPSCs during the reprogramming process, which is critical for induced pluripotency. We found that SIRT2KD in human fibroblasts significantly increases hiPSC generation while SIRT2OE prominently inhibits it. Regulation of SIRT1 expression is also critical for induced pluripotency but in the opposite direction: SIRT1OE significantly increases hiPSC generation whereas SIRT1KD robustly interferes with it. In line with their opposite direction of expression, it appears that SIRT1 and SIRT2 regulate induced pluripotency through distinct mechanisms and targets. For instance, our results highlight that acetylation levels and activities of glycolytic enzymes (for example, aldolase, PGK1, enolase, and GAPDH) are robustly regulated by SIRT2, but not SIRT1. In agreement with our results, previous studies showed upregulation of SIRT1 in hPSCs[29,30] and SIRT1's important roles for generation of mouse iPSCs[30,37]. In addition, the study by Si *et al.*[31] showed that SIRT2 is upregulated during *in vitro* differentiation of mouse ESCs and SIRT2KD promotes mesoderm and endoderm lineages while compromising ectoderm differentiation. In contrast, our results show that SIRT2 regulates more fundamental stem cell functions such as metabolism, cell survival/death, and pluripotent differentiation potential in hPSCs. The different functional role(s) of SIRT2 between these two studies possibly reflect species differences (mouse versus human). Another possibility is that SIRT2 has distinct functional role(s) for different stem cell state. Unlike primed hPSCs, mouse ESCs are at a naive pluripotent state and energetically bivalent[9]. Thus, further investigations are needed to determine whether SIRT2 (and/or SIRT1) distinctively regulate stem cell function in naive and primed pluripotent stem cells.

Importantly, we found multiple lines of evidence strongly suggesting that SIRT2 is a key regulator of metabolic reprogramming (Warburg-like effect) during human induced pluripotency, and critically regulates stem cell functions. Firstly, SIRT2OE in hESCs robustly altered acetylation and enzymatic activities of glycolytic enzymes, significantly compromising glycolytic metabolism. Secondly, SIRT2OE in hPSCs caused enhanced OXPHOS and reduced glycolysis, leading to significantly reduced cell proliferation, at least in part, by increased apoptotic cell death via enhanced production of ROS. In addition, SIRT2OE in hPSCs leads to enhanced pluripotent differentiation potential that is accompanied by a further reduction of lactate production. Thirdly, SIRT2KD in human fibroblasts robustly increased acetylation levels and activities of glycolytic enzymes, leading to prominent metabolic switch from OXPHOS to glycolytic metabolism. Fourthly, SIRT2KD together with the introduction of reprogramming factors into human fibroblasts more rapidly and effectively induced metabolic switch compared to reprogramming factors alone, resulting in more efficient hiPSC generation. In contrast, altered expression of SIRT1 did not directly influence the metabolic status, further supporting that SIRT1 and SIRT2 regulate the reprogramming process via distinct mechanisms. Taken together, our data indicate that altered levels of SIRT2 during induced pluripotency and differentiation regulate OXPHOS and glycolysis in opposite directions, thus facilitating the metabolic switches.

While SIRT2's regulation of glycolysis appears to be linked to acetylation levels of glycolytic enzymes and their activities, at present it is unknown how OXPHOS is regulated. Although it is possible that SIRT2 regulates OXPHOS through PGC1α, a master regulator of mitochondrial biogenesis[41], its precise regulatory mechanism(s) await further investigation. Notably, SIRT2 is the only sirtuin residing primarily in the cytoplasm[18,19], and this may provide a unique advantage to directly control metabolic reprogramming by regulating glycolytic enzymes which also reside in the cytoplasm.

Our finding that there is a direct correlation between acetylation levels and enzymatic activities is surprising because it was suggested that acetylation is inhibitory to the activities of most enzymes[42]. For instance, a glycolytic enzyme, phosphoglycerate mutase, was reported to be stimulated through deacetylation by SIRT2 (ref. 43). However, other studies showed that the same enzyme's activity is downregulated by SIRT1 or SIRT2 (refs 44,45). In addition, a recent study showed that GAPDH is activated by acetylation of its K254 residue[46]. Furthermore, increasing GapA acetylation in Salmonella by Pat acetylase treatment increased its glycolysis activity[16]. Thus, the functional effect of acetylation appears to be enzyme- and perhaps lysine-specific. To further validate our findings, we performed LC-MS/MS analyses of aldolase A. We identified K111 and K322 as specific SIRT2 target sites and found that deacetylation of K322 by SIRT2 critically inhibits the enzyme activity of aldolase A. K322 resides on an outside surface with unknown functional domain, and our functional data will provide useful insights into this important enzyme and its regulation in diseases such as cancer.

Finally, we found that SIRT2 is suppressed by miR-200c, a miRNA induced in pluripotent stem cells by Oct4 (ref. 40), via binding sites in the sirtuin gene coding sequence. This miRNA enhances metabolic reprogramming via SIRT2 suppression and this appears to be a critical step of induced pluripotency (Fig. 8g). Indeed, enforced SIRT2OE is highly inhibitory to iPSC reprogramming in human cells. It should be of interest to determine whether this regulation of metabolism by the miR-200c–SIRT2 axis is also important for other types of stem cells (for example, adult stem cells, naive pluripotent stem cells, and cancer stem cells). A defect in this pathway could lead to abnormal stem cell functions and compromised development in embryos or dysfunctional tissues in adults. Further, manipulation of the metabolic control of cell fate and function via the miR-200c–SIRT2 axis may aid translational approaches that use stem cells for regenerative medicine and cell replacement therapy.

METHODS

Cell culture

Human BJ dermal fibroblasts (hDF) and HEK293T cells were purchased from ATCC and grown in Dulbecco's modified Minimal Essential Medium (DMEM) supplemented with 2mM L-glutamine, 10% fetal bovine serum (FBS), 100Uml^{-1} penicillin and 100 μgml^{-1} streptomycin (all from Invitrogen). For iPSC induction, DMEM/F-12 medium supplemented with 2mM L-glutamine, 1mM β-mercaptoethanol, 1x non-essential amino acids (NEAA), 20% knockout serum replacement (KSR), 100Uml^{-1} penicillin, 100 μgml^{-1} streptomycin and 10 ngml^{-1} basic fibroblast growth factor (bFGF; all from Invitrogen) was used as the

reprogramming medium. Two hESC lines (H7(WA-07) and H9(WA-09)) and hiPSC line iPS-DF19-9-11T (iPS DF19-9-11T. H; termed hiPSC-2) were obtained from WiCell Institute. All hPSC lines were maintained in Essential 8 medium (Invitrogen) using Matrigel Matrix (Corning Life Sciences) and passaged using 0.5mM EDTA (Invitrogen) for gentle dissociation. No cell lines used in this study were found in the database of commonly misidentified cell lines that is maintained by ICLAC and NCBI Biosample. All cell lines were authenticated by Interspecies Determination (Isoenzyme Analysis and STR analysis) by the providing company and were routinely tested for mycoplasma detection using a Venor GeM Mycoplasma Detection Kit (Sigma-Aldrich).

Plasmid construction and lentivirus production

Human SIRT1 and SIRT2 coding sequences were PCR-amplified from hESCs (H9) and hDFs, respectively, then cloned into the pGEM-T Easy vector (Promega). The 2A sequence of the Thoseaasigna virus (T2A)-linked EGFP was amplified from plasmid pCXLE-EGFP (#27082; Addgene) by RT-PCR and cloned into the pGEM-T Easy vector. The SIRT1 and SIRT2 fragments were then cut off from the corresponding vectors and inserted into the pGEM-T-T2A-EGFP to generate pGEM-T-SIRT1-T2A-EGFP and pGEM-T-SIRT2-T2A-EGFP, respectively. The identity of the SIRT1-T2A-EGFP and SIRT2-T2A-EGFP constructs was confirmed by sequencing. Subsequently, they were introduced into the EcoRI site of the FUW-tetO vector (Addgene). Human AldoA-Myc constructs, the AldoA fragment was PCR-amplified from H9 hESCs, and then cloned into the pcDNA3.1-Myc/His vector (Invitrogen). For the psicheck-2 constructs, the CDS fragments were cloned downstream of the Renilla luciferase open reading frame. AldoA point mutations were generated by site-directed mutagenesis using a QuickChange II XL Site-Directed Mutagenesis kit (Agilent Technologies).

FUW-tetO-based lentiviral vectors containing the other individual reprogramming factors for Oct4 (#20726), Sox2 (#20724), Klf4 (#20725) or c-Myc (#20723) were purchased from Addgene. The polycistronic human STEMCCA lentiviral vector[47] was kindly provided by G. Mostoslavsky (Boston University). Genetic knockdown of SIRT1 or SIRT2 was carried out using lentiviral shRNA plasmids targeting human SIRT1 (RHS3979-201750186, RHS3979-201750188, RHS3979-201750189, and RHS3979-201750190) or human SIRT2 (RHS3979-201797165, RHS3979-201768981, RHS3979-201768982, RHS3979-201768983, RHS3979-201768984, and RHS3979-201768985) that were obtained from GE Healthcare Dharmacon.

For lentivirus production, lentiviral vectors were co-transfected with packaging plasmids into 293T cells, maintained in DMEM supplemented with 10% FBS, using Lipofectamine 2000 (Invitrogen) according to the manufacturer's instruction. Supernatants containing lentivirus were harvested 48 h after transfection and filtered using 0.45 μm Millex-HV (Millipore) filters to remove cell debris.

Human iPSC induction

Human iPSCs were generated using lentiviral particles from inducible lentiviral vectors or STEMCCA vectors to introduce the OSKM factors (Oct4, Sox2, Klf4, and c-Myc) into

fibroblasts[48]. ES-like colonies formed after 3 weeks of viral infection and the observed ES-like colonies were handpicked and transferred onto mouse feeder cells (MEF)-plated or on Matrigel-coated tissue culture plates to generate iPSC lines. iPSC colonies were mechanically picked until iPSC lines were established. One of the established iPSC clone (termed hiPSC-1) were used for further analyses. Authentication of the hiPSC-1 cell line was performed on the basis of pluripotent gene expression.

Web-based meta-analysis

Microarray datasets from five independent studies (GSE28633; ref. 24, GSE18265; ref. 25, GSE20013; ref. 26, GSE39144 (http://www.ncbi.nlm.nih.gov/geo/query/acc.cgi?acc=GSE39144), and GSE9709; ref. 27) of hESCs and/or hiPSCs against various sets of differentiated cell types (for example, fibroblasts, neurons or endothelial cells) were analysed using GEO2R (https://www.ncbi.nlm.nih.gov/geo/geo2r) to identify acetylation-modulating factor(s) whose expression is significantly different in hPSCs compared to their differentiated counterparts[28]. Of 40,000–50,000 primers, corresponding to mRNA transcripts, only the top 20% of mRNA transcripts were selected as a cutoff range to validate significance, based on *P* values. Each gene expression in a given database was further monitored across multiple groups of hPSCs to determine gene expression changes.

Live cell metabolic analysis

Oxygen consumption rate (OCR) and extracellular acidification rates (ECAR) were measured using the XFp8 or XF24 analyser (Agilent Technologies) according to the manufacturer's instructions. Briefly, cells were plated into wells of an XF cell culture microplate and incubated at 37 °C in a CO_2 incubator for 24 h to ensure attachment. The assay was started after cells were equilibrated for 1 h in XF assay medium supplemented with 10mM glucose, 5mM sodium pyruvate and 2mM glutamine in a non-CO_2 incubator. Mitochondrial activity between hDFs and hESCs/parental hDFs and iPSCs were monitored through sequential injections of 1 μM oligomycin, 0.3 μM FCCP and 1 μM rotenone/antimycin A to calculate basal respiration rates (baseline OCR—rotenone/antimycin A OCR), ATP dependent (basal respiration rate—oligomycin OCR), maximum respiration (FCCP OCR—rotenone/antimycin A OCR), and oxidative reserve (maximum respiration rate—basal respiration rate). Glycolytic processes were measured by serial injections of 10mM glucose, 1 μM oligomycin, and 100mM 2-deoxyglucose to calculate basal glycolytic rate, glycolytic capacity (in response to oligomycin), and glycolytic reserve (glycolytic capacity—basal rate). Each plotted value was normalized to total protein quantified using a Bradford protein assay (Bio-Rad).

Immunoprecipitation

For immunoprecipitation assays, hESCs and hDFs lysates were incubated with specific antibodies against acetyl-Lys (Cell Signaling Technology, catalogue No. 9441, 1:100), aldolase (Santa Cruz Technology, catalogue No. sc-12059, 1:100), enolase (Cell Signaling Technology, catalogue No. 3810, 1:50), PGK1 (Santa Cruz Technology, catalogue No. sc-130335, clone No. 14, 1:100) or GAPDH (Santa Cruz Technology, catalogue No. sc-32233, clone No. 6C5, 1:50) at 4 °C overnight. After addition of protein A/G UltraLink resin, samples were incubated at 4 °C for 2 h. Beads were washed three times with PBS and

proteins were released from the beads by boiling in SDS-sample loading buffer and analysed by SDS–PAGE.

Liquid chromatography mass spectrometry (LC-MS/MS)

For identification of acetylated proteins, hESCs or hDFs (control) were grown in 100mm dishes up to 60–70% confluence. Cells were collected, washed with PBS and lysed (50mM Tris-HCl, pH 7.4, 150mM NaCl, 1mM EDTA, 1mM EGTA, 0.5% NP-40, 1% SDS, and protease inhibitor cocktail). Whole cell lysate from hESCs and hDFs were incubated for 10 min on ice followed by centrifugation at 14,000*g* for 15 min at 4 °C. Supernatants were collected and pellets were discarded. Protein concentrations were determined using the BCA assay (Pierce) using bovine serum albumin (BSA) as standard. For immunoprecipitation assays, 500 μg of hESC and hDFs lysates were incubated with anti-acetyl-Lys antibody (Cell Signaling Technology, catalogue No. 9441, 1:100) at 4 °C for overnight. After addition of Protein A/GUltraLink resin, samples were incubated at 4 °C for 2 h. Beads were washed three times with PBS and proteins were released from the beads by addition of SDS-sample loading buffer. The eluted proteins were analysed by SDS–PAGE and the gel stained with Coomassie Blue. For LC-MS/MS analyses, the gel was de-stained and bands cut and processed as follows. Briefly, acetylated proteins bands were divided into 10mm sections and subjected to in-gel digestion with trypsin. The tryptic digests were separated by online reversed-phase chromatography using a Thermo Scientific Eazy nano LC II UHPLC equipped with an autosampler using a reversed-phase peptide trap EASY-Column(100 μm inner diameter, 2 cm length) and a reversed-phase analytical EASY-Column (75 μm inner diameter, 10 cm length, 3 μm particle size), both from Thermo Scientific, followed by electrospray ionization using a 30 μm (i.d.) nanobore stainless steel online emitter (Thermo Scientific) and a voltage set at 2.6V, at a flow rate of 300 nl min^{-1}. The chromatography system was coupled in line with an LTQ-Orbitrap mass spectrometer. Spectra were searched against the Human IPI v3.7 DB using the Sorcerer 2 IDA Sequest-based search algorithm, and comparative analysis of proteins identified in this study was performed using Scaffold 4. LC-MS/MS analysis was performed at the Biopolymers & Proteomics Core Facility of the David H. Koch Institute at MIT and at the Medicinal Bioconvergence Research Center at Seoul National University. To compare protein acetylation between hESCs and hDFs, we quantified the acetylated proteins in both samples based on spectral counts. The spectral counts were first normalized to ensure that average spectral counts per protein were the same in the two data sets[49]. A G test was used to judge statistical significance of protein abundance differences[50]. Briefly, the G value of each protein was calculated as follows,

$$G=2(S_1 \times \ln[S_1/((S_1+S_2)/2)]+S_2 \times \ln[S_2/((S_1+S_2)/2)])$$

where S_1 and S_2 are the detected spectral counts of a given protein in any of two samples for comparison. Although the theoretical distribution of G values is complex, these values approximately fit to the χ^2 distribution (1 degree of freedom), allowing the calculation of related P values[50]. For identification of acetylation sites on AldoA, we pulled down Myc-conjugated AldoA proteins from 293T cells infected with AldoA-Myc-overexpressing plasmid together with empty or SIRT2KD plasmid by immunoprecipitation with Myc

antibody (Sigma-Aldrich, catalogue No. 11667149001, clone No. 9E10, 1:200). The AldoA-Myc band was excised, digested with chymotrypsin, and analysed using an LTQ-Orbitrap ion-trap mass spectrometer from Thermo Scientific (Taplin Mass Spectrometry Facility, Harvard University (https://taplin.med.harvard.edu/home)).

Western blot analysis

Samples (50 μg) were loaded onto a 12% SDS–PAGE and separated by electrophoresis followed by transfer onto a piece of Immun-Blot PVDF membrane (Bio-Rad). After transfer, the membrane was blocked at room temperature with Tris-buffered saline (TBS) containing 0.1% Tween-20 and 5% (w/v) skim milk for 3–5 h and then incubated overnight at 4 °C with primary antibody. The membrane was washed three times with TBS containing 0.05% Tween-20 (TBST) and then incubated for 2 h with horseradish peroxidase (HRP)-conjugated goat anti-mouse IgG (Santa Cruz Biotechnology, 1:1,000) or goat anti-rabbit IgG (Invitrogen, 1:3,000). After washing twice with TBST and once with TBS, bound antibodies were detected by chemiluminescence using the SuperSignal West Pico kit (Pierce). Antibodies against acetyl-Lys (Catalogue No. 9441, 1:1,000) and Enolase (Catalogue No. 3810, 1:1,000) were purchased from Cell Signaling Technology, β-actin (Catalogue No. ab8227, 1:1,000), α-tubulin (Catalogue No. ab4074, 1:1,000), acetylated-α-tubulin (Catalogue No. ab24610, clone No. 6-11B-1, 1:1,000), SIRT1 (Catalogue No. ab32441, clone No. E104, 1:1,000), and SIRT2 (Catalogue No. ab51023, clone No. EP1668Y, 1:1,000) from Abcam, Aldolase A (Catalogue No. sc-12059, 1:1,000), PGK1 (Catalogue No. sc-130335, clone No. 14, 1:1,000), GAPDH (Catalogue No. sc-32233, clone No. 6C5, 1:1,000) from Santa Cruz Biotechnology. We used HRP-conjugated Veriblot for IP secondary antibody (Abcam, catalogue No. ab131366, 1:500) to facilitate detection of immunoprecipitated proteins without co-detecting the IgG heavy and light chains. The PVDF membrane was stripped by washing three times with TBST followed by incubation at 50 °C for 30 min with shaking in stripping buffer (62.5mM Tris-HCl, pH 6.7, 100mM β-mercaptoethanol, and 2% SDS). After incubation, the membrane was washed several times with TBST. Stripped membranes were blocked and probed with primary and secondary antibodies as previously described.

Immunofluorescence

For immunofluorescence assays, cells were immediately fixed (2% formaldehyde, 100mM KCl, 200mM sucrose, 1mM EGTA, 1mM $MgCl_2$, 10mM PIPES, pH 6.8) for 10 min, washed with PBS and then treated with permeabilization buffer (0.2% Triton X-100, 100mM KCl, 200mM sucrose, 1mM EGTA, 1mM $MgCl_2$, 10mM PIPES, pH 6.8) for 10 min. Cells were washed with PBS three times and incubated with blocking solution containing 3% BSA in PBS for 15 min. Cells were washed with PBS three times and incubated with primary antibodies in blocking solution at 4 °C overnight. Oct4 (Catalogue No. sc-5279, clone No. C-10, 1:500) and Nanog (Catalogue No. sc-33759, 1:500) antibodies were obtained from Santa Cruz Biotechnologies, SSEA4 (Catalogue No. MAB4304, clone No. MC-813-70, 1:500), TRA-1-60 (Catalogue No. MAB4360, clone No. TRA-1-60, 1:500) and Tyrosine hydroxylase (TH, catalogue No. AB1542, 1:1,000) antibodies from EMD Millipore, Otx2 (Catalogue No. AF1979, 1:500), Sox17 (Catalogue No. AF1924, 1:500) and Brachyury (Catalogue No. AF2085, 1:500) antibodies from R&D Systems, class III β-

tubulin (Tuj1, catalogue No. MMS-435P, clone No. TUJ1, 1:500) antibody from Covance. Cells were washed with PBS three times and incubated with goat anti-mouse Alexa 488, donkey anti-rabbit Alexa 568 or donkey anti-sheep Alexa 568 (Invitrogen, 1:300) in blocking solution. After washing with PBS, nuclei were stained with Hoechst33342 (Invitrogen). Each image was examined using a confocal laser-scanning microscope (Olympus America).

Quantitative reverse transcription polymerase chain reaction (qRT-PCR)

Total RNA was extracted from cells by using the Direct-zol RNA purification Kit (Zymo Research) and cDNA was synthesized using the ThermoScript RT-PCR system (Invitrogen). For quantitative analyses, qRT-PCR (Bio-Rad) were performed using SsoAdvanced SYBR Green supermix (Bio-Rad) with target genes specific primers. The expression level of each gene is shown as a relative value following normalization against that of the β-actin gene. Primers used in this study are listed in Supplementary Table 8.

ATP determination assay

Cellular ATP concentration was measured using an ATP determination kit (Molecular Probe). Cells (iPSCs and parental hDFs/hESCs and hDFs) were washed three times with PBS and lysed by addition of water and boiled for 5 min. Cell lysates were collected by centrifugation for 15 min at 4 °C. ATP chemiluminescent detection was performed using firefly luciferase and luciferin and measured by a SpectraMax L (Molecular Devices). Cell lysates protein concentrations were determined using the Bradford assay (Bio-Rad) and relative luminescent units were normalized according to protein concentrations.

Neuronal and spontaneous differentiation

Neuronal differentiation was performed as described previously with slight modifications[51]. Briefly, hESCs were dissociated and plated on bacterial dishes in hESC medium without bFGF for 1 week to allow formation of embryoid bodies (EB). EBs were allowed to attach to tissue culture dish and neuronal precursors were selected by incubation in DMEM/F-12 medium supplemented with 2mM L-glutamine, Insulin-Transferrin-Selenium-G (Invitrogen), and fibronectin (Sigma-Aldrich) for 30 days. hESCs and hiPSCs *in vitro* spontaneous differentiations were performed by culturing in serum-free ITSFn medium for different periods of time up to 12 days without EB formation.

Fluorescence-based competition assay

Fluorescence-based competition assay was performed as described previously with slight modifications[37,38]. Briefly, GFP expressing hESCs (GFP) or SIRT2 (and GFP)-inducible hESCs (SIRT2) were mixed with wild-type hESCs (GFP^-) and cultured in Matrigel-coated 6-well plates. Every five days (one passage) cells were dissociated using accutase (Sigma-Aldrich) and replated. At each passage, the proportion of GFP^+/GFP^- cells was measured by flow cytometry on a BD Accuri flow cytometer using the Accuri C6 data analysis software. Analyses were carried out for six consecutive passages.

Enzyme activity assay

Enzyme activity of aldolase, enolase, and GAPDH was measured using an enzymatic colorimetric assay kit (All from Biovision) according to the manufacturer's instructions.

Proliferation assay

Cells were detached using accutase for 10 min and suspended in ESC medium and counted using a haemocytometer. An equal number of cells (1×10^4 cells/well) were seeded on Matrigel-coated 12-well plates. The total number of cells per well was determined at 2, 4, 6 days post-seeding using a haemocytometer.

Annexin V staining

For apoptosis analysis, cells were washed twice with cold PBS, and then stained with Annexin V-PE and 7-AAD (559763; BD Biosciences), and analysed by flow cytometer.

Luciferase reporter assay

We used the Promega dual luciferase assay kit to perform the luciferase assay according to the manufacturer's instructions. In brief, cell lysates were analysed for luciferase activity using the dual luciferase system and two luciferase enzymes, one (from *Renilla reniformis*) containing the experimental target sequence and another (from firefly) containing the control. The Renilla/firefly luciferase ratios were normalized against the empty psicheck-2 vector and averaged over six replicates.

Cellular ROS measurements

Intracellular ROS levels were determined using a CellROX Deep Red Oxidative Stress Reagent (C10422; Life technologies) according to the manufacturer's instructions.

Lactate assay

Extracellular lactate production was measured using L-Lactate assay kit (700510; Cayman Chemical) according to the manufacturer's instructions.

Statistics and reproducibility

Data were analysed using GraphPad Prism 5.0.1 software (GraphPad Software) and are presented as mean with s.e.m. or s.d. (as indicated in figure legends). Statistic tests were performed and *P* value thresholds were obtained using GraphPad 5.0.1. Multiple groups were tested using analysis of variance (ANOVA) and comparisons between two groups were performed using two-tailed unpaired Student's *t*-test. Statistically significant differences are indicated as follows: $^{*}P < 0.05$; $^{**}P < 0.01$; $^{***}P < 0.005$; $^{****}P < 0.001$. Representative figures are shown in Figs 1a,d,f,i, 2a–c,e,f, 3a, 4e, 5f, 7e,f,i and 8b,e and Supplementary Figs 1a–d,g, 4c and 8e,f. Each experiment was repeated independently: 2 repeats (Figs 1e and 5g and Supplementary Fig. 7f), 3 repeats (Figs 1a,c,d,f–i, 2, 3a,c,d, 4a–f,h, 5, 6, 7d–f,i and 8a,b,d–f and Supplementary Figs 1a–d,f,g, 4, 5e,f, 6, 7a–e and 8b–h), 4 repeats (Fig. 7a–c,g,h and Supplementary Fig. 1e), 5 repeats (Fig. 4g).

Data availability

Previously published data sets are available under accession numbers GSE28633, GSE18265, GSE20013, GSE39144, and GSE9709. LC-MS/MS results used in this study have been provided in Supplementary Tables 1 and 2. All raw mass spectrometry proteomics data reported in this study have been deposited to the ProteomeXchange Consortium via the PRIDE partner repository with the data set identifier PXD006036. Source data for Figs 1c,e,g,h, 2d,g, 3c,d, 4a–d,f–h, 5a–e,g, 6a–k, 7a–i and 8a,d,f, and Supplementary Figs 1d–f, 4b,d, 5e,f, 6a–h, 7a–f and 8b–h have been provided in Supplementary Table 9. Unprocessed western blots, including two repeat experiments for each blot, have been provided for Figs 1a,d,i, 2b,c,e,f, 3a and 8b,e, and Supplementary Fig. 1d,g in Supplementary Fig. 9. All other data supporting the findings of this study are available from the corresponding author upon request.

Supplementary Material

Refer to Web version on PubMed Central for supplementary material.

Acknowledgments

This work was supported by NIH grants (NS084869, NS070577, and GM101420) and the National Research Foundation of Korea (2011-0030043). The authors are grateful to members of the Kim laboratory for critical discussions.

References

1. Warburg O, Wind F, Negelein E. The metabolism of tumors in the body. J Gen Physiol. 1927; 8:519–530. [PubMed: 19872213]
2. Warburg O. On the origin of cancer cells. Science. 1956; 123:309–314. [PubMed: 13298683]
3. Rafalski VA, Mancini E, Brunet A. Energy metabolism and energy-sensing pathways in mammalian embryonic and adult stem cell fate. J Cell Sci. 2012; 125:5597–5608. [PubMed: 23420198]
4. Ito K, Suda T. Metabolic requirements for the maintenance of self-renewing stem cells. Nat Rev Mol Cell Biol. 2014; 15:243–256. [PubMed: 24651542]
5. Burgess RJ, Agathocleous M, Morrison SJ. Metabolic regulation of stem cell function. J Intern Med. 2014; 276:12–24. [PubMed: 24697828]
6. Zhang J, Nuebel E, Daley GQ, Koehler CM, Teitell MA. Metabolic regulation in pluripotent stem cells during reprogramming and self-renewal. Cell Stem Cell. 2012; 11:589–595. [PubMed: 23122286]
7. Folmes CD, Dzeja PP, Nelson TJ, Terzic A. Metabolic plasticity in stem cell homeostasis and differentiation. Cell Stem Cell. 2012; 11:596–606. [PubMed: 23122287]
8. Zhang J, et al. UCP2 regulates energy metabolism and differentiation potential of human pluripotent stem cells. EMBO J. 2011; 30:4860–4873. [PubMed: 22085932]
9. Zhou W, et al. HIF1α induced switch from bivalent to exclusively glycolytic metabolism during ESC-to-EpiSC/hESC transition. EMBO J. 2012; 31:2103–2116. [PubMed: 22446391]
10. Varum S, et al. Energy metabolism in human pluripotent stem cells and their differentiated counterparts. PLoS ONE. 2011; 6:e20914. [PubMed: 21698063]
11. Folmes CD, et al. Somatic oxidative bioenergetics transitions into pluripotency-dependent glycolysis to facilitate nuclear reprogramming. Cell Metab. 2011; 14:264–271. [PubMed: 21803296]
12. Moussaieff A, et al. Glycolysis-mediated changes in acetyl-CoA and histone acetylation control the early differentiation of embryonic stem cells. Cell Metab. 2015; 21:392–402. [PubMed: 25738455]

13. Panopoulos AD, et al. The metabolome of induced pluripotent stem cells reveals metabolic changes occurring in somatic cell reprogramming. Cell Res. 2012; 22:168–177. [PubMed: 22064701]
14. Kim SC, et al. Substrate and functional diversity of lysine acetylation revealed by a proteomics survey. Mol Cell. 2006; 23:607–618. [PubMed: 16916647]
15. Zhao S, et al. Regulation of cellular metabolism by protein lysine acetylation. Science. 2010; 327:1000–1004. [PubMed: 20167786]
16. Wang Q, et al. Acetylation of metabolic enzymes coordinates carbon source utilization and metabolic flux. Science. 2010; 327:1004–1007. [PubMed: 20167787]
17. Guarente L. The logic linking protein acetylation and metabolism. Cell Metab. 2011; 14:151–153. [PubMed: 21803285]
18. Guarente L, Franklin H. Epstein Lecture: Sirtuins, aging, and medicine. N Engl J Med. 2011; 364:2235–2244. [PubMed: 21651395]
19. Finkel T, Deng CX, Mostoslavsky R. Recent progress in the biology and physiology of sirtuins. Nature. 2009; 460:587–591. [PubMed: 19641587]
20. Gatenby RA, Gillies RJ. Why do cancers have high aerobic glycolysis? Nat Rev Cancer. 2004; 4:891–899. [PubMed: 15516961]
21. Mathieu J, et al. Hypoxia-inducible factors have distinct and stage-specific roles during reprogramming of human cells to pluripotency. Cell Stem Cell. 2014; 14:592–605. [PubMed: 24656769]
22. Prigione A, et al. HIF1α modulates cell fate reprogramming through early glycolytic shift and upregulation of PDK1-3 and PKM2. Stem Cells. 2014; 32:364–376. [PubMed: 24123565]
23. North BJ, Marshall BL, Borra MT, Denu JM, Verdin E. The human Sir2 ortholog, SIRT2, is an NAD+-dependent tubulin deacetylase. Mol Cell. 2003; 11:437–444. [PubMed: 12620231]
24. Fathi A, et al. Comprehensive gene expression analysis of human embryonic stem cells during differentiation into neural cells. PLoS ONE. 2011; 6:e22856. [PubMed: 21829537]
25. Assou S, et al. A meta-analysis of human embryonic stem cells transcriptome integrated into a web-based expression atlas. Stem Cells. 2007; 25:961–973. [PubMed: 17204602]
26. Li Z, et al. Functional and transcriptional characterization of human embryonic stem cell-derived endothelial cells for treatment of myocardial infarction. PLoS ONE. 2009; 4:e8443. [PubMed: 20046878]
27. Masaki H, et al. Heterogeneity of pluripotent marker gene expression in colonies generated in human iPS cell induction culture. Stem Cell Res. 2007; 1:105–115. [PubMed: 19383391]
28. Barrett T, et al. NCBI GEO: archive for functional genomics data sets–update. Nucleic Acids Res. 2013; 41:D991–D995. [PubMed: 23193258]
29. Calvanese V, et al. Sirtuin 1 regulation of developmental genes during differentiation of stem cells. Proc Natl Acad Sci USA. 2010; 107:13736–13741. [PubMed: 20631301]
30. Lee YL, et al. Sirtuin 1 facilitates generation of induced pluripotent stem cells from mouse embryonic fibroblasts through the miR-34a and p53 pathways. PLoS ONE. 2012; 7:e45633. [PubMed: 23029150]
31. Si X, et al. Activation of GSK3β by Sirt2 is required for early lineage commitment of mouse embryonic stem cell. PLoS ONE. 2013; 8:e76699. [PubMed: 24204656]
32. Marchler-Bauer A, et al. CDD: NCBI's conserved domain database. Nucleic Acids Res. 2015; 43:D222–D226. [PubMed: 25414356]
33. Gamblin SJ, et al. Activity and specificity of human aldolases. J Mol Biol. 1991; 219:573–576. [PubMed: 2056525]
34. Zhang J, et al. Measuring energy metabolism in cultured cells, including human pluripotent stem cells and differentiated cells. Nat Protoc. 2012; 7:1068–1085. [PubMed: 22576106]
35. Park KS, et al. Transcription elongation factor Tcea3 regulates the pluripotent differentiation potential of mouse embryonic stem cells via the Lefty1-Nodal-Smad2 pathway. Stem Cells. 2013; 31:282–292. [PubMed: 23169579]
36. Ivanova N, et al. Dissecting self-renewal in stem cells with RNA interference. Nature. 2006; 442:533–538. [PubMed: 16767105]

37. Mu WL, et al. Sox2 deacetylation by Sirt1 is involved in mouse somatic reprogramming. Stem Cells. 2015; 33:2135–2147. [PubMed: 25940188]
38. Miranda KC, et al. A pattern-based method for the identification of MicroRNA binding sites and their corresponding heteroduplexes. Cell. 2006; 126:1203–1217. [PubMed: 16990141]
39. Suh MR, et al. Human embryonic stem cells express a unique set of microRNAs. Dev Biol. 2004; 270:488–498. [PubMed: 15183728]
40. Wang G, et al. Critical regulation of miR-200/ZEB2 pathway in Oct4/Sox2-induced mesenchymal-to-epithelial transition and induced pluripotent stem cell generation. Proc Natl Acad Sci USA. 2013; 110:2858–2863. [PubMed: 23386720]
41. Gomes P, Outeiro TF, Cavadas C. Emerging role of Sirtuin 2 in the regulation of mammalian metabolism. Trends Pharmacol Sci. 2015; 36:756–768. [PubMed: 26538315]
42. Xiong Y, Guan KL. Mechanistic insights into the regulation of metabolic enzymes by acetylation. J Cell Biol. 2012; 198:155–164. [PubMed: 22826120]
43. Xu Y, et al. Oxidative stress activates SIRT2 to deacetylate and stimulate phosphoglycerate mutase. Cancer Res. 2014; 74:3630–3642. [PubMed: 24786789]
44. Hallows WC, Yu W, Denu JM. Regulation of glycolytic enzyme phosphoglycerate mutase-1 by Sirt1 protein-mediated deacetylation. J Biol Chem. 2012; 287:3850–3858. [PubMed: 22157007]
45. Tsusaka T, et al. Deacetylation of phosphoglycerate mutase in its distinct central region by SIRT2 down-regulates its enzymatic activity. Genes Cells. 2014; 19:766–777. [PubMed: 25195573]
46. Li T. Glyceraldehyde-3-phosphate dehydrogenase is activated by lysine 254 acetylation in response to glucose signal. J Biol Chem. 2014; 289:3775–3785. [PubMed: 24362262]
47. Somers A, et al. Generation of transgene-free lung disease-specific human induced pluripotent stem cells using a single excisable lentiviral stem cell cassette. Stem Cells. 2010; 28:1728–1740. [PubMed: 20715179]
48. Takahashi K, et al. Induction of pluripotent stem cells from adult human fibroblasts by defined factors. Cell. 2007; 131:861–872. [PubMed: 18035408]
49. Kislinger T, et al. Global survey of organ and organelle protein expression in mouse: combined proteomic and transcriptomic profiling. Cell. 2006; 125:173–186. [PubMed: 16615898]
50. Zhou JY, et al. Galectin-3 is a candidate biomarker for amyotrophic lateral sclerosis: discovery by a proteomics approach. J Proteome Res. 2010; 9:5133–5141. [PubMed: 20698585]
51. Kim D, et al. Generation of human induced pluripotent stem cells by direct delivery of reprogramming proteins. Cell Stem Cell. 2009; 4:472–476. [PubMed: 19481515]

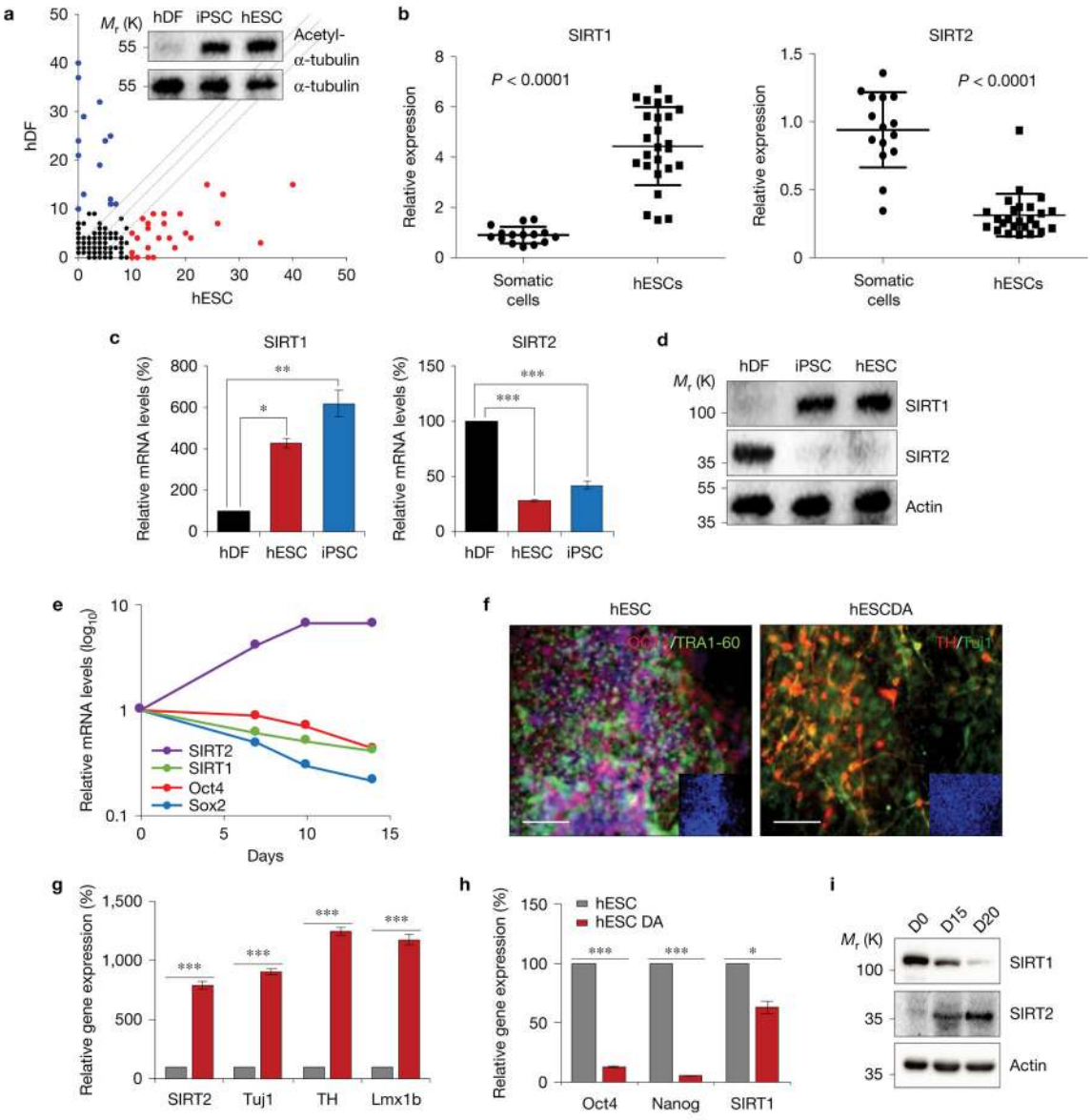

Figure 1.

SIRT2 downregulation and SIRT1 upregulation is a molecular signature of human pluripotency. (**a**) Immunoprecipitation of hDF and hESCs proteins using antibodies against acetyl-Lys, following LC-MS/MS analyses to identify acetylated proteins. Red and blue dots represent hyperacetylated proteins in hESCs and in hDFs, respectively. (**b**) Mean value scatter plot of relative expression levels of SIRT1 and SIRT2 in hESC lines ($n = 25$) and normal somatic cell lines ($n = 15$) using results from a database search (http://www.nextbio.com). All cell line information is shown in Supplementary Table 5. (Mean ± s.e.m., two-tailed unpaired Student's *t*-test.) (**c**) SIRT1 and SIRT2 expression from hDFs, iPSCs and hESCs was determined by qRT-PCR. (Mean ± s.e.m., $n = 3$ biologically independent experiments, $^{*}P < 0.05$; $^{**}P < 0.01$; $^{***}P < 0.005$, one-way ANOVA with Newman–Keuls post-test.) (**d**) Protein levels of SIRT1 and SIRT2. (**e**) Relative mRNA levels of SIRT1, SIRT2, Oct4 and SOX2 during *in vitro* differentiation of hESCs. ($n = 2$

biologically independent experiments.) (**f**) Immunofluorescence assays of pluripotency markers (Oct4 and Tra-1-60) and neuronal markers (TH and Tuj1) before and after *in vitro* DA differentiation, respectively. Hoechst was used to show nucleus. Scale bar, 100 μm. (**g**,**h**) Gene expression levels of DA neuronal markers (TH, Lmx1b, and Tuj1) (**g**) and pluripotency markers (**h**) are shown along with those of SIRT1 and SIRT2. (Mean ± s.e.m., n=3 biologically independent experiments, $^{*}P < 0.05$; $^{***}P < 0.005$, two-tailed unpaired Student's t-test.) (**i**) SIRT1 and SIRT2 protein levels during *in vitro* DA differentiation. Statistics source data are in Supplementary Table 9. Unprocessed original scans of blots **a**,**d**,**i** are shown in Supplementary Fig. 9.

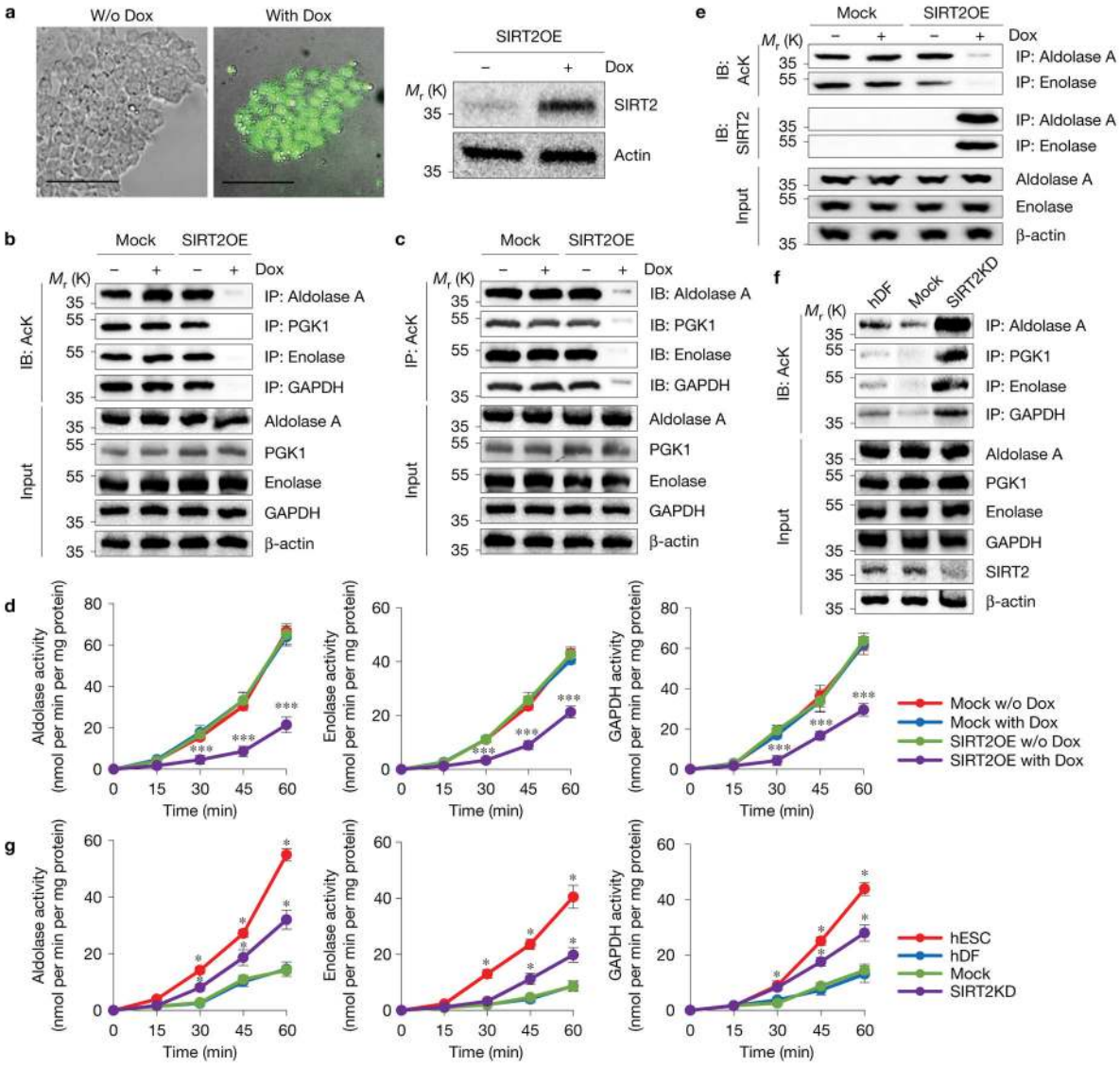

Figure 2.

SIRT2 regulates acetylation and enzymatic activity of glycolytic enzymes. (**a**) Left: representative pictures of inducible SIRT2-GFP H9 hESCs with or without doxycycline (Dox). Scale bar, 100 μm. Right: the efficiency of SIRT2 overexpression was confirmed by western blotting with SIRT2-specific antibody. (**b**–**d**) Total protein extracts from wild-type (mock) and inducible SIRT2-GFP hESCs (SIRT2OE) with or without Dox were immunoprecipitated with anti-Aldolase A, anti-PGK1, anti-Enolase or anti-GAPDH antibodies (**b**) or anti-acetyl-Lys (**c**). Acetylation levels of each enzyme were assessed by western blotting with an anti-acetyl-Lys antibody (**b**) or each specific antibody (**c**). Enzymatic activities in each extracts are shown in **d**. Western blotting of Aldolase A, PGK1, Enolase, GAPDH, and β-actin using equal amounts of extracts are shown as the control (input). (Mean ± s.d., n=3 biologically independent experiments, $^{***}P < 0.005$, two-way ANOVA with Bonferroni post-test.) (**e**) Total proteins from mock and SIRT2OE with or without Dox were immunoprecipitated using anti-Aldolase A or anti-Enolase antibodies and

western blotting was performed with anti-acetyl-Lys or anti-SIRT2 antibodies. Aldolase A, Enolase, and β-actin western blotting of whole cell lysate (Input) from wild-type and SIRT2-GFP hESCs were used as control of equal protein concentration for the IP. (**f**,**g**) Total protein extracts from mock and SIRT2 knockdown (KD) hDFs were immunoprecipitated by anti-Aldolase A, anti-PGK1, anti-Enolase or anti-GAPDH antibodies. Acetylation levels and enzyme activity of Aldolase A, PGK1, Enolase or GAPDH were determined by western blotting with anti-acetyl-Lys antibody (**f**) and enzymatic assays (**g**), respectively. Aldolase A, PGK1, Enolase, GAPDH, and β-actin western blotting of whole cell lysate (input) from WT and SIRT2KD hDFs were used as control of equal concentration for the IP and enzymatic activity assays. (Mean ± s.d. shown. n=3 biologically independent experiments, $^{*}P < 0.05$, two-way ANOVA with Bonferroni post-test.) Statistics source data are in Supplementary Table 9. Unprocessed original scans of blots **a**–**c**,**e**,**f** are shown in Supplementary Fig. 9.

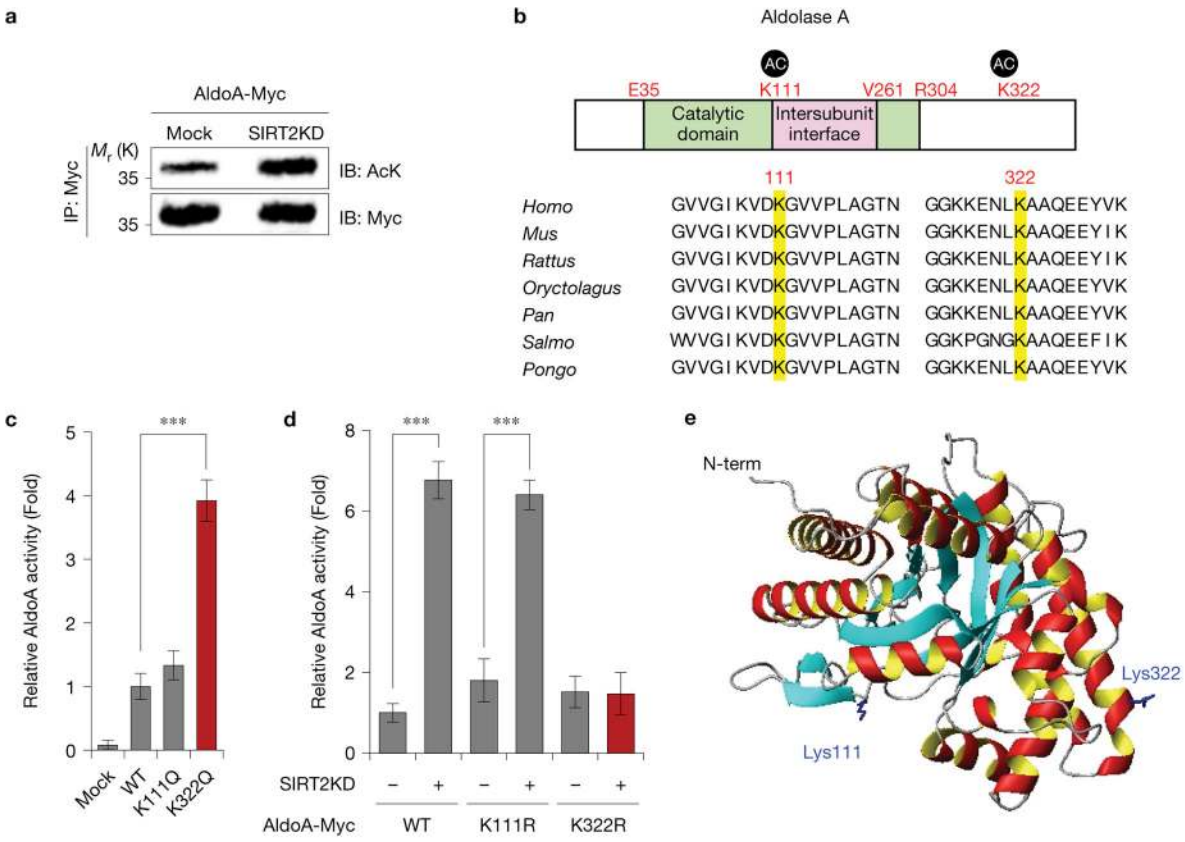

Figure 3.

Acetylation status of K322 regulates AldoA activity. (**a**) Western blotting shows that AldoA-Myc is highly acetylated in SIRT2KD 293T cells although total proteins are unchanged. (**b**) Sequence alignment of putative acetylation sites (K111 and K322) from different species. (**c**) Myc-tagged AldoA, AldoA^{K111Q}, and AldoA^{K322Q} were each expressed in hDFs. AldoA proteins were purified by IP with a Myc antibody, and specific activity for AldoA was determined. (Mean ± s.d., n=3 biologically independent experiments, $^{***}P < 0.005$, one-way ANOVA with Bonferroni post-test.) (**d**) Myc-tagged AldoA, AldoA^{K111R}, and AldoA^{K322R} were each expressed in hDFs co-expressing SIRT2 shRNA (SIRT2KD). AldoA proteins were purified by IP with Myc antibody, and specific activity for AldoA was determined. (Mean ± s.d., n=3 biologically independent experiments, $^{***}P < 0.005$, one-way ANOVA with Bonferroni post-test.) (**e**) Crystal structure model of human AldoA (Protein Data Bank code: 1ALD). Statistics source data are in Supplementary Table 9. Unprocessed original scans of blots **a** are shown in Supplementary Fig. 9.

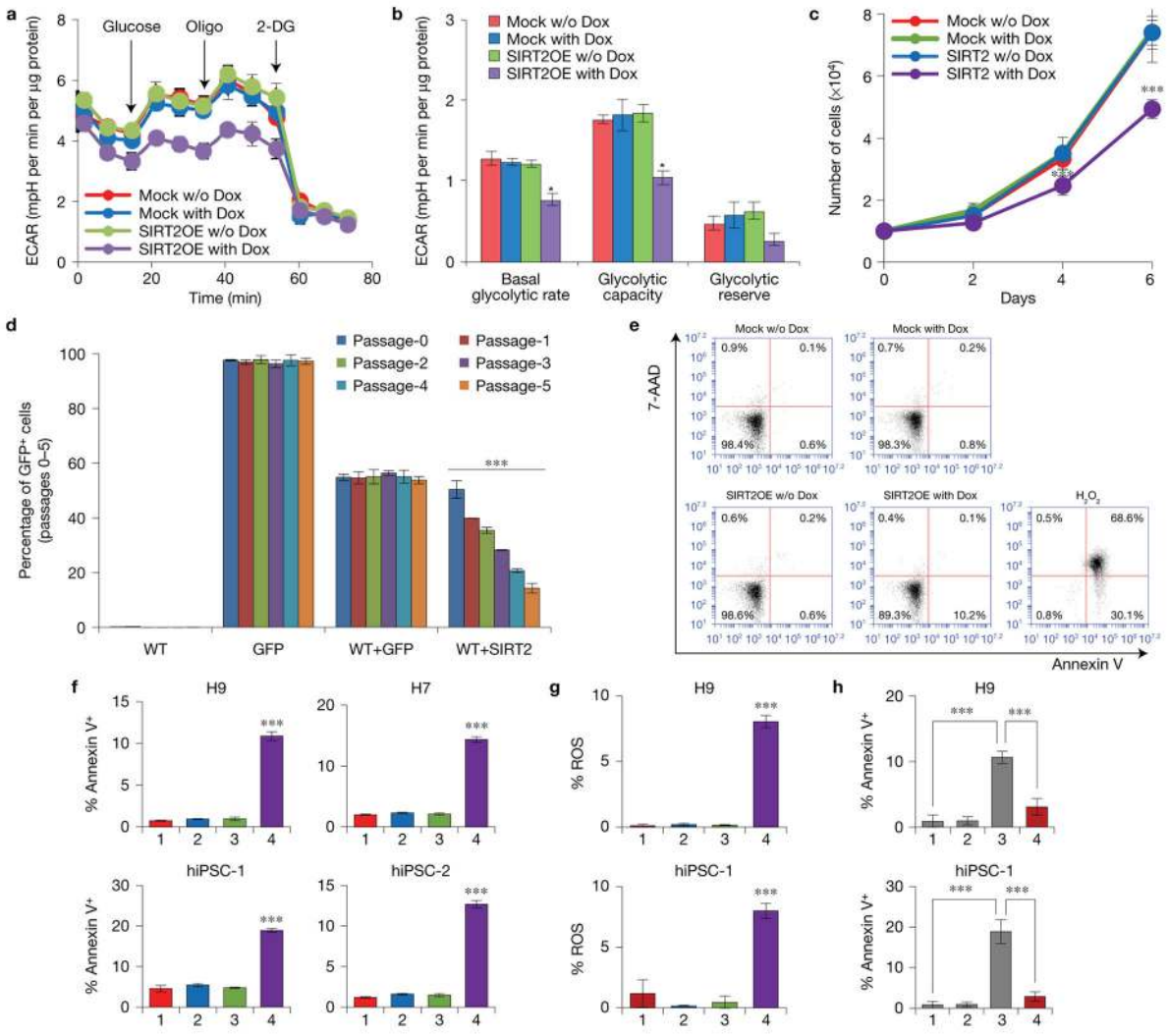

Figure 4.

SIRT2 influences metabolism and cell survival of hPSCs. (**a**) Glycolytic bioenergetics of wild-type (mock) and inducible SIRT2-GFP H9 hESCs (SIRT2OE) with or without Dox were assessed using the Seahorse XF analyser. Mean ± s.d. shown. n=3 biologically independent experiments. (**b**) Basal glycolytic rate, glycolytic capacity and glycolytic reserve from mock and SIRT2OE with or without Dox shown in **a**. (Mean ± s.d., n=3 biologically independent experiments, $^{*}P < 0.05$, one-way ANOVA with Bonferroni post-test.) (**c**) Cell proliferation of mock and SIRT2OE H9 hESCs with or without Dox was analysed by determining cell numbers every two days under ESC culture condition. (Mean ± s.d., $n = 3$ biologically independent experiments, $^{***}P < 0.005$, two-way ANOVA with Bonferroni post-test.) (**d**) GFP-positive (GFP^{+}) WT and SIRT2 H9 hESCs with or without Dox were mixed at a ratio of 1:1 with GFP-negative (GFP^{-}) hESCs, respectively. The GFP^{+}/GFP^{-} ratios were measured at each passage. (Mean ± s.d., n=3 biologically independent experiments, $^{***}P < 0.005$, two-way ANOVA with Bonferroni post-test.) (**e**) Apoptotic population of mock and SIRT2OE H9 hESCs with or without Dox for three days under ESC culture conditions measured by Annexin V/7-AAD staining. (**f**) Quantification of

Annexin V positive cells in mock and SIRT2OE hESC lines (H9 and H7) and two iPSC lines (iPSC-1 and iPSC-2) with or without Dox. 1: Mock w/o Dox, 2: Mock with Dox, 3: SIRT2OE w/o Dox, 4: SIRT2OE with Dox. (Mean ± s.d., n=3 biologically independent experiments, $^{***}P < 0.005$, one-way ANOVA with Bonferroni post-test.) (**g**) Intracellular ROS levels of mock and SIRT2OE hPSCs (H9 and hiPSC-1) with or without Dox. 1: Mock w/o Dox, 2: Mock with Dox, 3: SIRT2OE w/o Dox, 4: SIRT2OE with Dox. (Mean ± s.d., n = 5 biologically independent experiments, $^{***}P < 0.005$, one-way ANOVA with Bonferroni post-test.) (**h**) Effect of antioxidant on cell death of hPSCs (H9 and hiPSC-1) by SIRT2OE with or without Dox. 1: Veh only, 2: NAC, 3: Dox+Veh, 4: Dox+NAC. (Mean ± s.d., n=3 biologically independent experiments, $^{***}P < 0.005$, one-way ANOVA with Bonferroni post-test.) Statistics source data are in Supplementary Table 9.

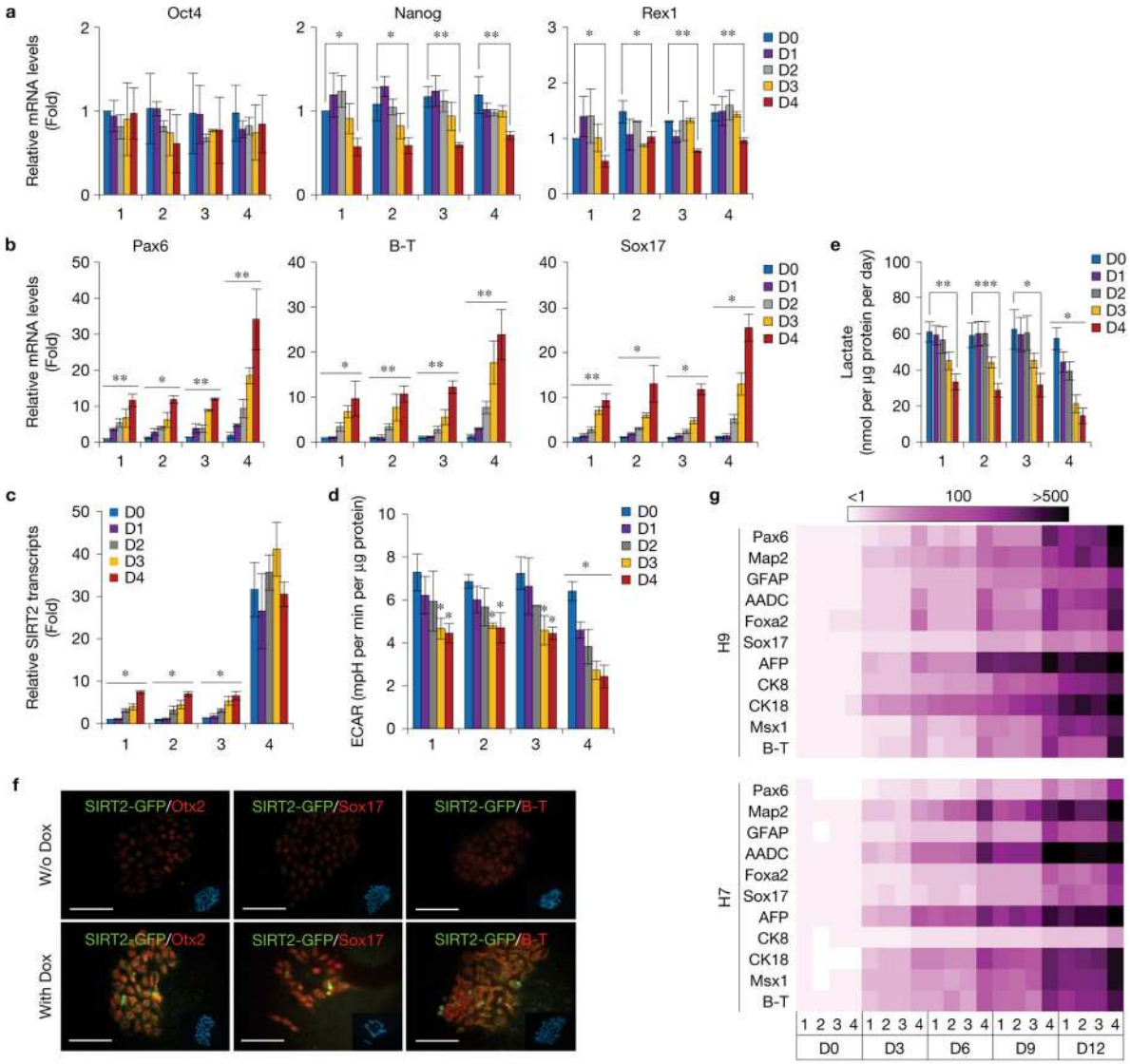

Figure 5.

SIRT2 influences metabolism during early *in vitro* differentiation of hESCs. (**a**,**b**) Inducible SIRT2OE H9 hESCs were induced to differentiate spontaneously by culturing in serum-free ITSFn medium for up to 4 days, and gene expression levels of pluripotency markers (Oct4, Nanog, and Rex1) (**a**) and early-differentiation markers (Pax6, Brachyury (B-T), and Sox17) (**b**) were determined by qRT-PCR. (Mean ± s.d., n=3 biologically independent experiments, $^{*}P < 0.05$; $^{**}P < 0.01$, one-way ANOVA with Bonferroni posttest.) (**c**) Expression level of SIRT2 in SIRT2OE H9 hESCs with or without Dox during early differentiation. (Mean ± s.d., n=3 biologically independent experiments, $^{*}P$ <0.05, one-way ANOVA with Bonferroni posttest.) (**d**) Glycolytic bioenergetics of mock and SIRT2OE H9 hESCs with or without Dox were assessed using the Seahorse XF analyser. (Mean ± s.d., n=3 biologically independent experiments, $^{*}P$ <0.05, one-way ANOVA with Bonferroni post-test.) (**e**) Extracellular lactate production of mock and SIRT2OE H9 hESCs with or without Dox. (Mean ± s.d., n=3 biologically independent experiments, $^{*}P < 0.05$; $^{**}P <$

0.01; $^{***}P < 0.005$, one-way ANOVA with Bonferroni post-test.) (**f**) SIRT2OE H9 hESCs were induced to differentiate spontaneously for 7 days, and differentiating cells were immunostained for the presence of lineage-specific markers for ectoderm (Otx2), endoderm (Sox17), and mesoderm (B-T). Scale bar, 100 μm. (**g**) Heatmaps depicting gene expression levels of markers representing ectoderm (Pax6, Map2, GFAP and AADC), endoderm (Foxa2, Sox17, AFP, CK8 and CK18), and mesoderm (Msx1 and B-T) in wild-type (Mock) and inducible SIRT2-GFP (SIRT2OE) H9 and H7 hESC lines with or without Dox differentiated for up to 12 days under differentiation condition. 1: Mock w/o Dox, 2: Mock with Dox, 3: SIRT2OE w/o Dox, 4: SIRT2OE with Dox. (n=2 biologically independent experiments.) Statistics source data are in Supplementary Table 9.

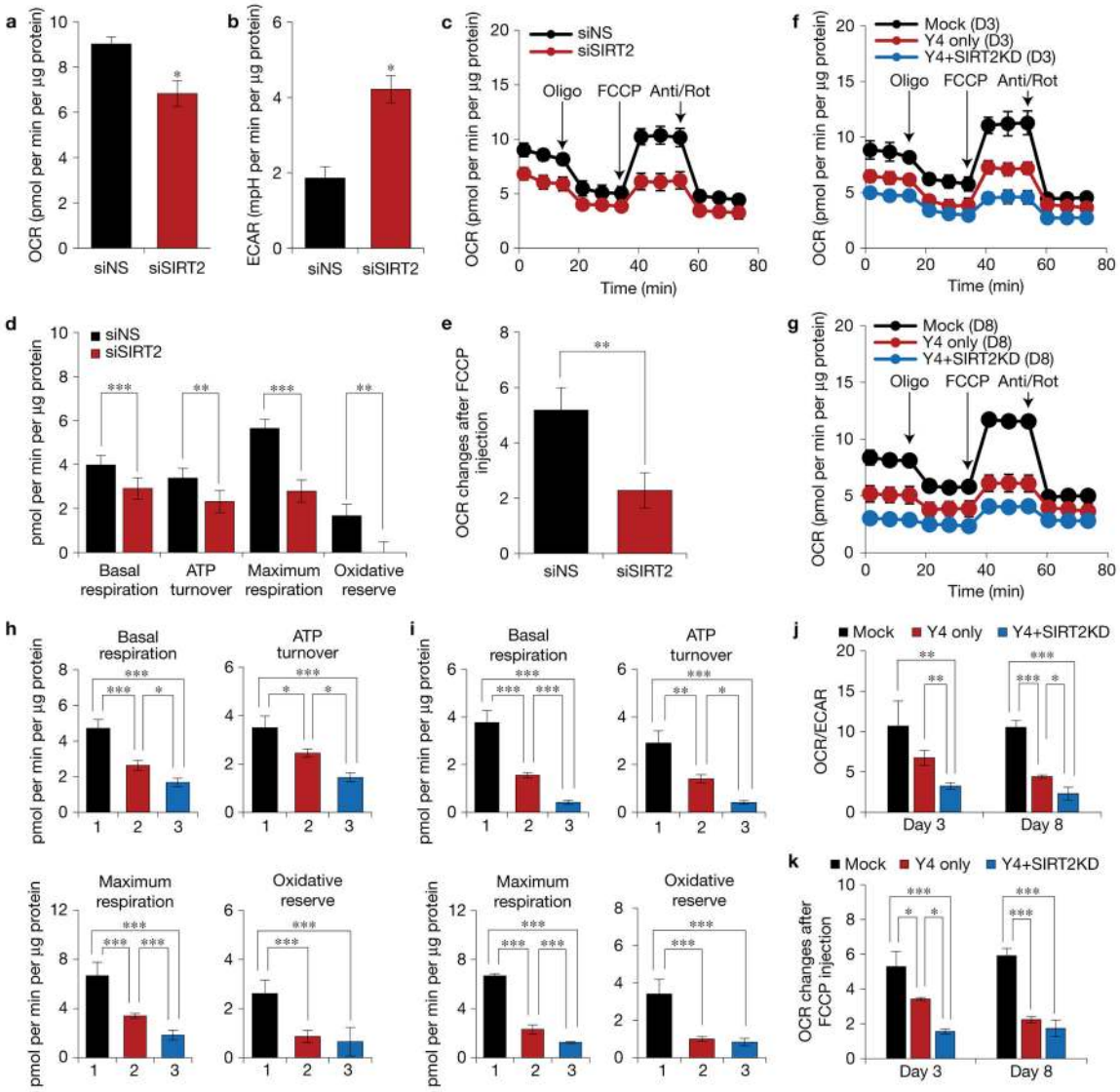

Figure 6.

SIRT2KD facilitates metabolic reprogramming in fibroblasts during the induced pluripotency. (**a**,**b**) Oxygen consumption rate (OCR) (**a**) and ECAR (**b**) of human fibroblasts (hDFs) infected with control (siNS) or SIRT2 siRNA (siSIRT2) at 3 days after transfection were assessed by XF analyser. (Mean ± s.d., $n = 3$ biologically independent experiments, $^{*}P < 0.05$, two-tailed unpaired Student's *t*-test.) (**c**) OXPHOS capacity of hDFs infected with siNS or siSIRT2 at 3 days after transfection. (Mean ± s.d., $n=3$ biologically independent experiments.) (**d**,**e**) Basal respiration, ATP turnover, maximum respiration, oxidative reserve (**d**) or relative OCR changes after FCCP injection (**e**) from siNS and siSIRT2 are shown in **c**. (Mean ± s.d., $n = 3$ biologically independent experiments, $^{**}P < 0.01$; $^{***}P < 0.005$, two-tailed unpaired Student's *t*-test.) (**f**,**g**) OCR were shown for hDFs infected with lentiviruses expressing four reprogramming factors (Y4) and/or SIRT2 knockdown (SIRT2KD) at 3 (**f**) or 8 (**g**) days after transfection. (Mean ± s.d., $n=3$ biologically independent experiments.) (**h**,**i**) Basal respiration, ATP turnover, maximum respiration, and oxidative reserve from Y4

and/or SIRT2KD at 3 (**h**) or 8 (**i**) days after transfection are shown in **f**,**g**. (Mean ± s.d., n=3 biologically independent experiments, $^{*}P$ <0.05; $^{**}P$ <0.01; $^{***}P$ <0.005, one-way ANOVA with Bonferroni posttest.) (**j**,**k**) OCR/ECAR ratio (**j**) or relative OCR changes after FCCP injection (**k**) from Y4 and/or SIRT2KD are shown in **f**,**g**. (Mean ± s.d., n = 3 biologically independent experiments, $^{*}P$ <0.05; $^{**}P$ <0.01; $^{***}P$ <0.005, one-way ANOVA with Bonferroni post-test.) Statistics source data are in Supplementary Table 9.

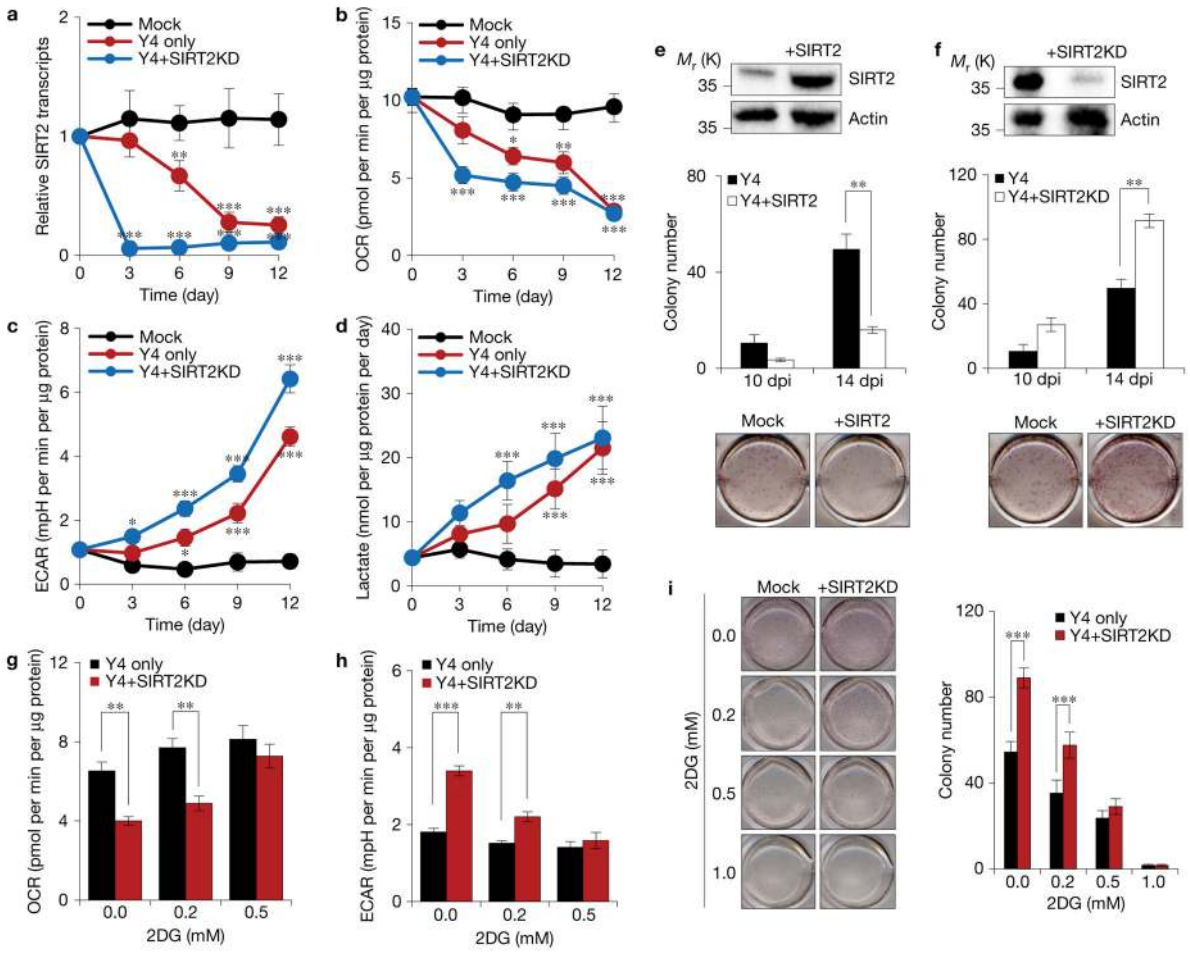

Figure 7.

SIRT2 influences somatic nuclear reprogramming through metabolic changes. (**a**) Time course of expression level of SIRT2 mRNA in hDFs infected with Y4 and/or SIRT2KD. (Mean ± s.d., $n = 4$ biologically independent experiments, $^{**}P < 0.01$; $^{***}P < 0.005$, two-way ANOVA with Bonferroni post-test.) (**b**,**c**) OCR (**b**) and ECAR (**c**) in hDFs infected with Y4 and/or SIRT2KD were assessed by XF analyser. (Mean ± s.d., n=4 biologically independent experiments, $^{*}P < 0.05$; $^{**}P < 0.01$; $^{***}P$<0.005, two-way ANOVA with Bonferroni post-test.) (**d**) Measurement of lactate production from hDFs infected with Y4 and/or SIRT2KD. (Mean ± s.d., n=3 biologically independent experiments, $^{***}P < 0.005$, two-way ANOVA with Bonferroni post-test.) (**e**,**f**) Effects of SIRT2OE or KD on iPSC generation. Upper: The efficiency of overexpression (**e**) or knockdown (**f**) was confirmed by western blotting with anti-SIRT2 antibody. Lower: Representative pictures of AP-positive colonies at 14 days post-infection (dpi). (Mean ± s.e.m., $n = 3$ biologically independent experiments, $^{**}P$<0.01, two-way ANOVA with Bonferroni post-test.) (**g**,**h**) Effects of glycolytic inhibitor, 2-deoxyglucose (2DG) on iPSC generation by Y4 and/or SIRT2KD at 8 days post-transduction were assessed by OCR (**g**) and ECAR (**h**). (Mean ± s.d., $n = 4$ biologically independent experiments, $^{**}P < 0.01$; $^{***}P$<0.005, two-way ANOVA with Bonferroni post-test.) (**i**) Effects of 2DG on iPSC generation by Y4 and/or SIRT2KD. Representative pictures

of AP-positive colonies at 14 days post-transduction. (Mean ± s.d., $n = 3$ biologically independent experiments, $^{***}P < 0.005$, two-way ANOVA with Bonferroni post-test.) Statistics source data are in Supplementary Table 9. Unprocessed original scans of blots **e**,**f** are shown in Supplementary Fig. 9.

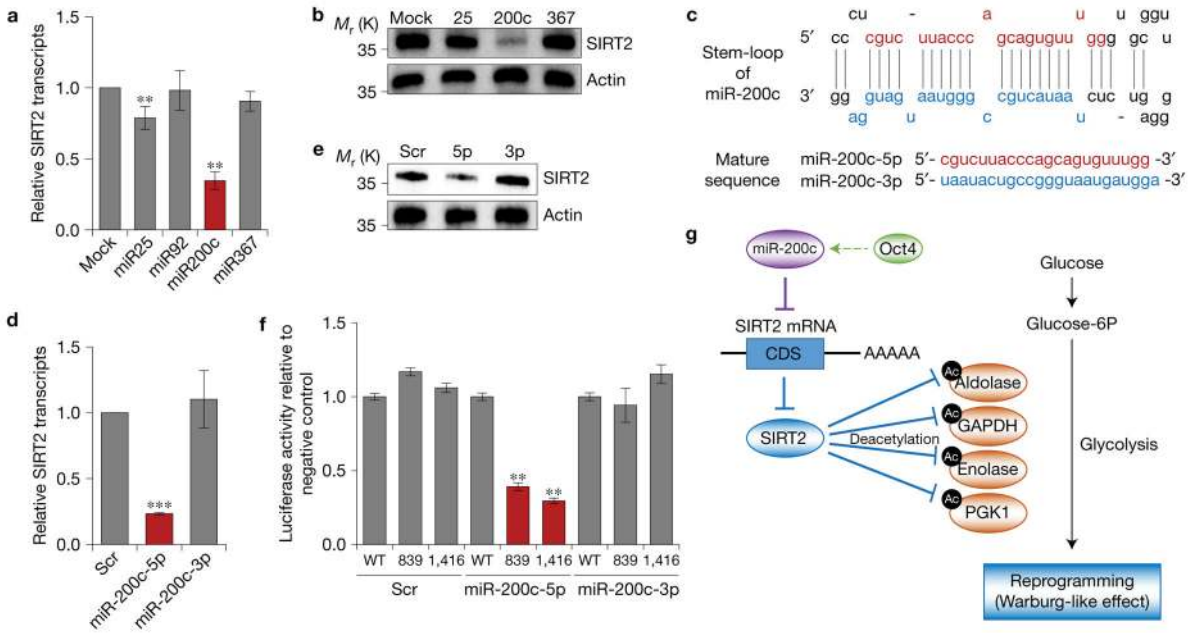

Figure 8.

miR-200c directly targets SIRT2. (**a**,**b**) Altered expression levels of SIRT2 by pre-miRNAs were analysed by qRT-PCR (**a**) or western blotting with SIRT2-specific antibody (**b**). (Mean ± s.d., n=3 biologically independent experiments, $^{**}P$ <0.01, one-way ANOVA with Bonferroni posttest.) (**c**) Sequences for stem loop of miR-200c (upper) and matured forms of miR-200c-5p and -3p (lower). (**d**,**e**) Altered expression levels of SIRT2 by miRNA mimics for control (Scr), miR-200c-5p (5p) and -3p (3p) were analysed by qRT-PCR (**d**) or western blotting with SIRT2-specific antibody (**e**). (Mean ± s.d., n=3 biologically independent experiments, $^{***}P$ <0.005, one-way ANOVA with Bonferroni post-test.) (**f**) Luciferase validation assays demonstrating the effect of miR-200c-5p on the CDS fragments of SIRT2 relative to control (Scr) in 293T cells. (Mean ± s.d., n = 3 biologically independent experiments, $^{**}P$ < 0.01, one-way ANOVA with Bonferroni post-test.) (**g**) Proposed model for miR-200c–SIRT2-glycolytic enzymes (aldolase, GAPDH, enolase, and PGK1) axis in regulating metabolic switch and somatic reprogramming. Statistics source data are in Supplementary Table 9. Unprocessed original scans of blots **b**,**e** are shown in Supplementary Fig. 9.